Chloroplast movement and positioning protein CHUP1 is required for focal immunity against *Phytophthora infestans*

Short title: Chloroplast movement protein is required for late blight immunity

Zachary Savage[1], Jessica L. Erickson[3,2], Jennifer Prautsch[2], Andrada I. Balmez[1], Yasin Tumtas[1], Enoch Lok Him Yuen[1], Johannes Stuttmann[4], Elisa Fantino[1], Cian Duggan[1], Camilla Molinari[1,4], Martin Schattat[2] & Tolga O. Bozkurt[1]

[1]Department of Life Sciences, Imperial College London, UK

[2]Department of Plant Physiology, Institute for Biology, Martin-Luther-Universität Halle-Wittenberg, Germany

[3]Leipnitz Institute for Plant Biochemistry, Halle, Germany

[4]Department of Plant Genetics, Institute for Biology, Martin-Luther-Universität Halle-Wittenberg, Germany

[5]The Sainsbury Laboratory, Norwich, UK

Abstract:

When a plant detects a pathogen, chloroplasts terminate photosynthetic activity and uptake vital roles in the immune system to help stave off infection, including the production of defense hormone precursors and antimicrobial reactive oxygen species. Additionally, chloroplasts associate with the nucleus and produce greater numbers of tubular extensions called stromules during immune challenge. We previously showed that during infection by the potato blight pathogen *Phytophthora infestan*s, chloroplasts accumulate at the pathogen haustoria, hyphal extensions that are accommodated within the host cell. However, the extent to which chloroplast positioning around haustoria, or at the nucleus, contributes to immunity during infection remains unknown. Here we show a striking increase in the susceptibility to *P. infestans* of *Nicotiana benthamiana* CRISPR knock-out lines lacking the chloroplast movement and anchoring gene, CHLOROPLAST UNUSUAL POSITIONING 1 (*CHUP1*). However, the positioning of chloroplasts around the haustorium or nucleus is not impaired in the absence of *CHUP1*. Further, loss of *CHUP1* leads to an extreme clustering of chloroplasts around the nucleus in the presence and absence of infection, showing that greater chloroplast-nucleus association does not necessarily equate to more robust immunity. While plants lacking *CHUP1* have reduced basal stromules, they are still able to induce stromules following immune stimulation, indicating that multiple populations of stromules exist. Lastly, we found that *CHUP1* is required for proper deposition of callose - a cell wall material implicated in pathogen penetration resistance - around *P. infestans* haustorium, but not for other core immune processes. Our results implicate chloroplasts in plant focal immunity and point to a key role of *CHUP1* in facilitating the deposition of defense material at the pathogen interface.

Introduction:

Filamentous pathogens such as oomycetes and fungi intimately interact with plant hosts, often through specialized infection structures that penetrate the host cells. Plants respond to pathogen penetration attempts with a spatially confined cell-autonomous defense response also known as focal immunity (Bozkurt et al., 2011; Dagdas et al., 2018; Duggan et al., 2021; Kwon et al., 2008). This involves significant cellular reorganization, involving organelle relocation, cell-wall reinforcements around contact sites through callose deposition, and polarized secretion of antimicrobials (Bozkurt et al., 2011, 2014; Ellinger et al., 2013; Heath et al., 1997; Savage et al., 2021). In addition to the secretory system and the nucleus, organelles such as chloroplasts and mitochondria accumulate around host cell penetration sites of fungal and oomycete pathogens (Fuchs et al., 2016; Savage et al., 2021). However, the extent to which these organelles contribute to focal immune responses remains to be elucidated.

Accumulating evidence points to key roles of chloroplasts in the deployment of various plant immune responses (Littlejohn et al., 2021). Upon immune activation by mitogen-activated protein kinases (MAPKs), chloroplasts terminate photosynthesis and activate a range of defense responses such as the production of reactive oxygen species (ROS) and defense hormones (Su et al., 2018). During the immune response, chloroplasts alter their morphology by extending stroma filled tubules, called stromules, that can make contacts with other membranes and organelles such as the nucleus (Caplan et al., 2015; Savage et al., 2021). In addition, chloroplasts cluster around the nucleus during immune stimulation (Ding et al., 2019), a response that is presumed to contribute towards plant defense, possibly through facilitating more efficient chloroplast-to-nucleus signaling.

Consistent with the emerging roles of chloroplast in immunity, an increasing number of effectors secreted by pathogens have been found to target chloroplast functions, whereas

plants monitor these potential threats using nucleotide-binding domain leucine-rich repeat containing (NLR) immune receptors (Gao et al., 2020; Jelenska et al., 2007; Pecrix et al., 2019; Petre et al., 2016; Xu et al., 2019; Zabala et al., 2015). For instance, the Irish potato famine pathogen *Phytophthora infestans* secretes the host translocated RXLR type of effector proteins, some of which can dampen chloroplast functions without being chloroplast localized (Gao et al., 2020; Savage et al., 2021). *P. infestans* can penetrate through host cells via specialized infection structures called haustoria that are implicated in delivery of effector proteins. Haustoria are excluded from the host cytoplasm through a newly synthesized plant-derived membrane called the extra-haustorial membrane (EHM) (S. Wang et al., 2017; Whisson et al., 2007). Remarkably, chloroplasts frequently gather around *P. infestans* haustorium, and in some cases associate with each other through stromules, forming clusters of chloroplasts (Savage et al., 2021). Occasionally, chloroplasts associate with the EHM through stromules that wrap around the haustoria (Savage et al., 2021). Given the range of antimicrobial and defense components produced by the chloroplasts, it is conceivable that the chloroplast position at the pathogen interface contributes to plant focal immune responses. However, the extent to which chloroplast positioning within the cell and around the haustorium contributes to plant immunity remains to be elucidated.

P. infestans and the solanaceous model plant species *Nicotiana benthamiana* are well established as an excellent pathosystem to study cell biology of plant responses to filamentous pathogens. As a pathogen, *P. infestans* is a useful agent to studying focal immune responses as it forms numerous haustoria that can be easily identified by confocal microscopy, which allows the monitoring of focal immune responses. *N. benthamiana* also lacks the specific NLR receptors with which to recognize *P. infestans*, rendering it partially susceptible to infection and therefore an excellent model to study the quantitative immune responses that contribute towards defense against this important pathogen. Furthermore, the lack of HR cell death enables live cell imaging of infected tissue, and thus the ability to dissect plant-pathogen interactions spatiotemporally within a single infected cell.

Here, we investigated the impact of chloroplast positioning during *P. infestans* infection by utilizing CRISPR knock-out lines of *N. benthamiana* lacking CHLOROPLAST UNUSUAL POSITIONING 1 (*CHUP1*), a gene essential for photorelocation responses and anchoring of chloroplasts to the plasma membrane (Oikawa et al., 2003, 2008; Suetsugu et al., 2016). We found a striking increase in susceptibility of *N. benthamiana* to *P. infestans* when *CHUP1* is knocked-down through virus induced gene silencing or knocked-out via CRISPR. In the absence of *CHUP1* chloroplast-haustoria association was not impaired, but we observed extreme clustering of chloroplasts around the nucleus. Plants lacking *CHUP1* had reduced basal stromules yet still induced them following immune stimuli, indicating that enhanced disease susceptibility is not caused by impaired stromule induction during infection. We lastly show that *chup1* knock-out plants are impaired in deposition of callose around *P. infestans* haustorium, but not in other core immune processes such MAPK triggered signaling and cell death as well as effector triggered HR cell death. We conclude that *CHUP1* contributes to plant focal immunity by somehow facilitating callose deposition at the pathogen penetration sites during intracellular infection.

Results:

Loss of *CHUP1* in *Nicotiana benthamiana* increases susceptibility to *Phytophthora infestans*

The role of chloroplasts in providing biochemical defense against pathogens is well established (Littlejohn et al., 2021). A less understood, yet emerging, aspect of chloroplast immunity is how the positioning and movement of epidermal chloroplasts during infection contributes to the immune response (Bozkurt et al., 2011; Ding et al., 2019; Irieda & Takano, 2021; Savage et al., 2021). We previously showed that during infection by the filamentous oomycete phytopathogen, *Phytophthora infestans*, epidermal chloroplasts of the model solanaceous plant, *Nicotiana benthamiana,* accumulate around the haustoria (Savage et al., 2021). To investigate this further, we performed infection assays (Fig. 1A) on *N. benthamiana* following down regulation of the chloroplast movement and anchoring gene, *CHUP1*. Silencing of the two identified *CHUP1* alleles (*NbCHUP1a and NbCHUP1b*) in transgenic *N. benthamiana* expressing GFP in the chloroplast stroma (CpGFP) through virus induced gene silencing (Fig. S1) led to significantly higher levels of *P. infestans* 88069td (red fluorescent strain) hyphal growth compared to the silencing control (Fig. 1B). To further validate these results, we generated CRISPR knock-out lines lacking *NbCHUP1a* and *NbCHUP1b* (*chup1* plants herein) from a transgenic parental line of *N. benthamiana* expressing chimeric protein FNR-EGFP which targets the plastid stroma (FNR herein) and performed infection assays with *P. infestans*. The mean hyphal growth of the pathogen per leaf (N = 14 infected leaves per genotype), which was inoculated in six different spots, was substantially higher in *chup1* plants compared to FNR control plants (Fig. 1C-D, Fig. S2), revealing that *chup1* plants are significantly more susceptible than the FNR control plants. These results implicate the chloroplast outer envelope protein CHUP1 in immunity against *P. infestans*, demonstrating that *CHUP1* contributes to immunity against an adapted pathogen

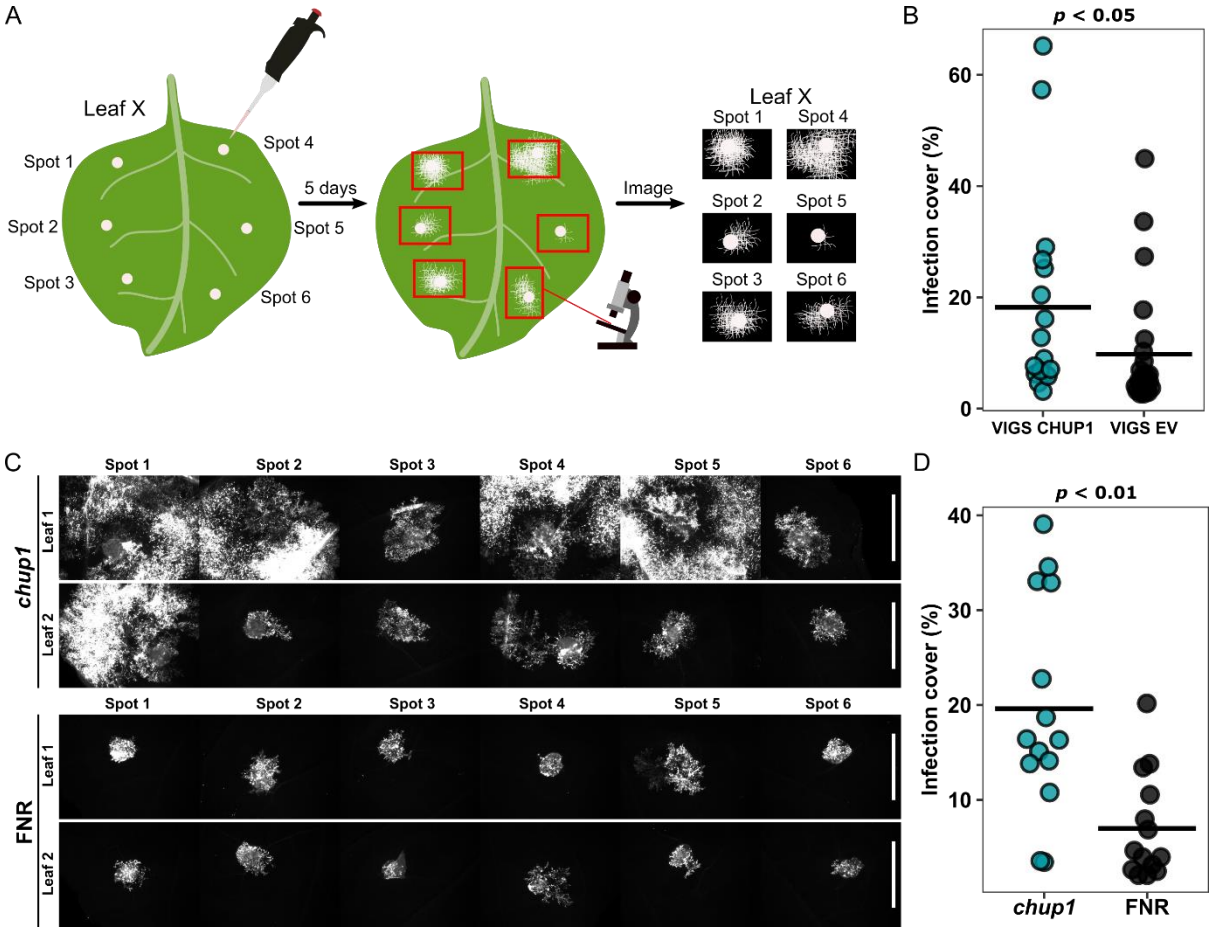

Figure 1: *CHUP1* positively contributes to immunity against *Phytophthora infestans*. (A) Cartoon representation of *P. infestans* infection assay method. Each different leaf is numbered and inoculated in six locations with a droplet of spore solution (spots 1-6). After five days, the infections are imaged by fluorescence stereomicroscopy. The area of hyphal growth (as a percentage of the image taken covered by hyphae) is automatically measured from each spot and averaged to give a single data point per leaf, derived from six inoculations. (B) Quantification of *P. infestans* 88069td hyphal growth infection assays of transgenic *N. benthamiana* expressing GFP in the chloroplast stroma (CpGFP) systemically silenced by VIGS for *CHUP1* or EV (empty vector control), shown as percentage of image area occupied by hyphae across all six inoculations of an infected leaf (*N* = 40 leaves per genotype). Cross bar represents the mean, p-value calculated from the Wilcoxon test. (C) Hyphal growth assays of *chup1* and FNR plants infected with *P. infestans*. Each leaf was inoculated with six droplets of spore solution (spots 1-6), two examples of infected leaves from each genotype shown (all infected leaves from the experiment shown in Fig. S2). Scale bars are 1 cm. (D) Quantification of hyphal growth infection assays as percentage of image area occupied by hyphae across all six inoculations of an infected leaf (*N* = 14 leaves per genotype). Cross bar represents the mean, p-value calculated from the Wilcoxon test.

Chloroplast positioning around the haustorium is not altered in *CHUP1* knock-outs

We previously showed that chloroplasts accumulate around *P. infestans* haustoria in infected epidermal cells, at rates higher than would be expected due to a random chance encounter, and in an actin dependent manner (Savage et al., 2021). Given that CHUP1 facilitates chloroplast movement and photorelocation during light avoidance responses in an actin dependent manner (Wada & Kong, 2018), we reasoned that this protein may also be responsible for chloroplast movement around haustoria during infection, impairment of which might account for the enhanced susceptibility of the *chup1* plants. To address this, we imaged *N. benthamiana* epidermal cells infected by *P. infestans* 88069td and quantified the number of haustoria associated with one or more chloroplasts in both *chup1* and FNR plants (Fig. 2A & B). However, we did not find any significant quantitative difference in chloroplast-haustoria association between *chup1* and FNR plants across 160 and 229 haustoria imaged respectively (Fig. 2C). The number of chloroplasts in the epidermal cells of the *chup1* and FNR plants did not vary significantly (Fig. S3A-B); we also measured the total chlorophyll concentration from leaves as an additional proxy for chloroplast numbers, again finding no difference between *chup1* and FNR plants (Fig. S3C). Further, the *chup1* plants did not show any major developmental defects, although they were slightly smaller than FNR control plants at a similar age (Fig. S3D). These results indicate that *CHUP1* is not essential for chloroplast positioning around the haustorium and the enhanced disease susceptibility of *chup1* knock-outs is not due to impaired chloroplast positioning at the pathogen interface or an abnormal number of chloroplasts in the cell.

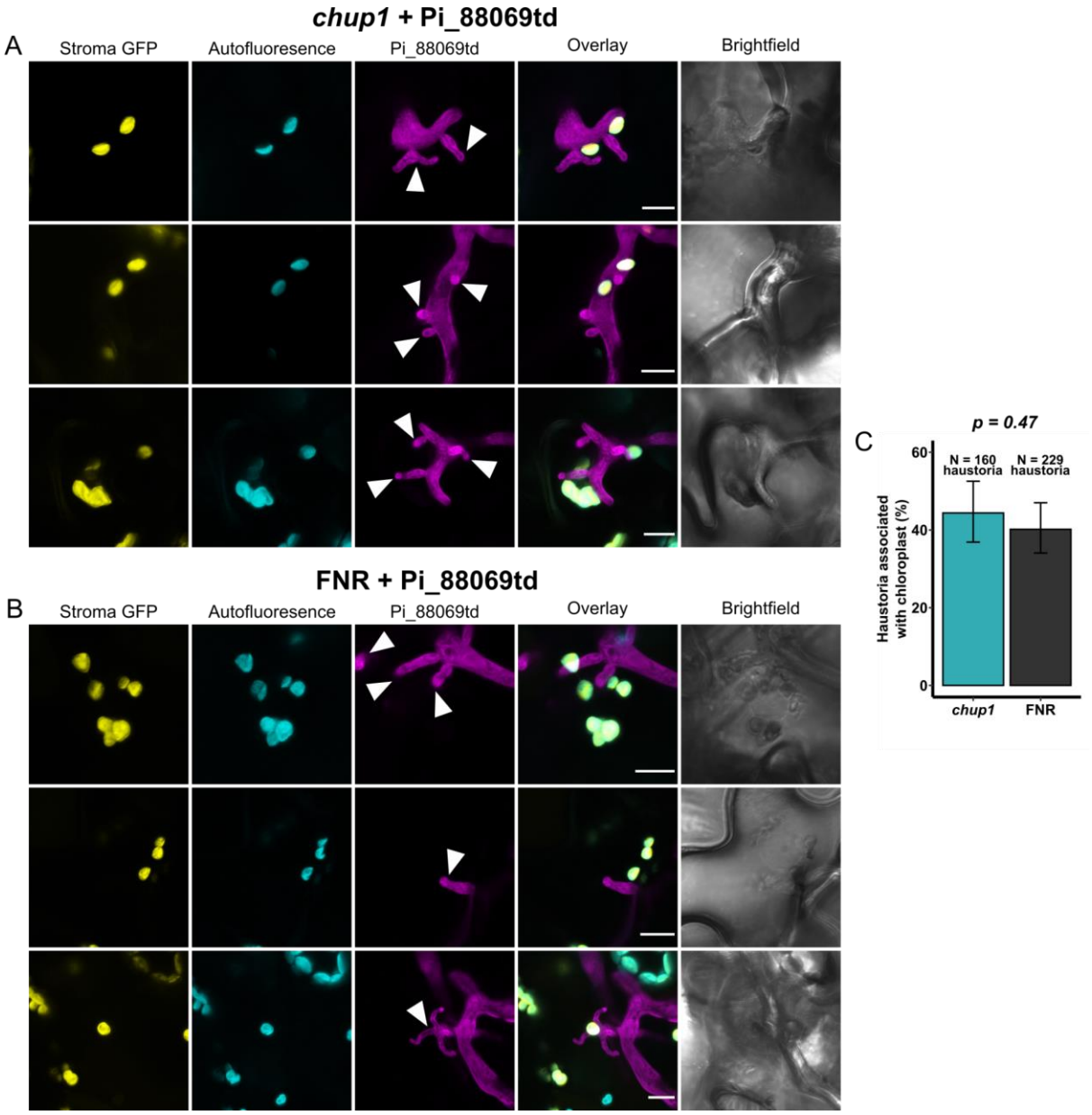

Figure 2: Chloroplast positioning at haustoria is unaffected by the loss of *CHUP1*. (A-B) Maximum projection confocal micrographs *N. benthamiana* epidermal cells during live infection by *P. infestans* 88069td (magenta), three days post inoculation, showing representative instances of chloroplast-haustoria association in: (A) *chup1* plants; (B) FNR control plants. Cyan shows chloroplast autofluorescence, yellow shows stroma targeted GFP. Intracellular haustoria marked by white arrowheads. Scale bars are 10 µm. (C) Quantified instances of chloroplast-haustoria association (as a percentage of total haustoria observed, *N* = 160 and *N* = 229 haustoria in *chup1* and FNR plants respectively). Error bars show 95% confidence intervals, *p*-value calculated from Fisher's Exact test. Chloroplast-haustoria association data was collected from the same set of micrographs shown and used in Figure 3 to assess stromules.

Chup1 knock-out plants have fewer basal stromules, but are not impaired in the induction of stromules by immune stimuli

Stromules are upregulated following infection by *P. infestans*, and following treatment by various PAMPs (Caplan et al., 2015; Savage et al., 2021), strongly suggesting they have some kind of immune function. Additionally, pathogen effectors are able to perturb stromule induction during infection, further suggesting that stromules play a role in the plant immune response (Erickson et al., 2018; Savage et al., 2021). Given that chloroplast-haustoria association was unaffected in the highly susceptible *chup1* plants, we next checked for the induction of stromules in these plants. In uninfected plants, we found levels of stromules to be consistently and significantly lower in the *chup1* plants compared to the FNR controls (Fig. 3A & B). This shows that *CHUP1* is required for stromule induction in uninfected plants, in contrast to a previous report by Caplan et al (2015) that VIGS silencing of *CHUP1* in *N. benthamiana* and Arabidopsis mutants lacking *CHUP1* had enhanced stromule formation. To determine whether the discrepancy in stromule numbers in the absence of *CHUP1* is due to differences in *N. benthamiana* versus Arabidopsis plants, we used the SALK_129128 T-DNA insertion line that results in a *CHUP1* knock-out, which we then transformed to express GFP localized to the stroma and mCherry localized to the nucleus (*A. thaliana chup1*-pn). In three independent lines of *A. thaliana chup1*-pn, we did not observe more stromules in epidermal plastids compared to the WT-pn control lines (Fig. S4A-B). Thus, we conclude that absence of *CHUP1* does not increase stromule frequency in contrast to what has been reported by Caplan et al (2015).

Because stromules are induced during *P. infestans* infection (Savage et al., 2021), we next investigated whether *chup1* plants are still able to induce stromules in response to pathogen challenge. Despite having reduced stromule levels in uninfected cells (Fig. 3A & B), *chup1* plants responded to infection with a stronger induction of stromules compared to the FNR control plants in three independent experiments (Fig. 3C & D). These results indicate that enhanced susceptibility of *chup1* plants is not due to a reduced capacity to produce stromules during infection. Furthermore, the ability of *chup1* plants to induce stromules during infection suggests that these (potentially immune related) stromules are not dependent on *CHUP1.* Higher levels of infection induced stromules in the *chup1* plants could be explained by an increased pathogen load (Fig. 1), triggering more plant immune signaling which in turn induces greater levels of stromules, alternatively the loss of *CHUP1* could be mechanistically relevant to the way stromules are produced during infection (which is currently not known).

Due to the biological complexity of live cell infection, such as differing amounts of pathogen growth and the secretion of pathogen effectors that interfere with plant processes, we tested for stromule induction using a heat-inactivated *P. infestans* derived extract that contains no live pathogen (Pi extract herein). In both the *chup1* and FNR plants, the infiltrated Pi extract significantly induced stromules compared to the water control in three independent biological replicates (Fig. 3E-G); both *chup1* and FNR produced similar levels of stromules during this response following 24 hr Pi extract treatment, whereas *chup1* plants had a stronger induction of stromules relative to the control treatments compared to the FNR plants (Fig. 3E-G). Therefore, we conclude that while knocking-out *chup1* suppresses levels of basal stromules, it does not inhibit the induction of immune related stromules, indicating that enhanced susceptibility of *chup1* plants is not due to impaired induction of stromules.

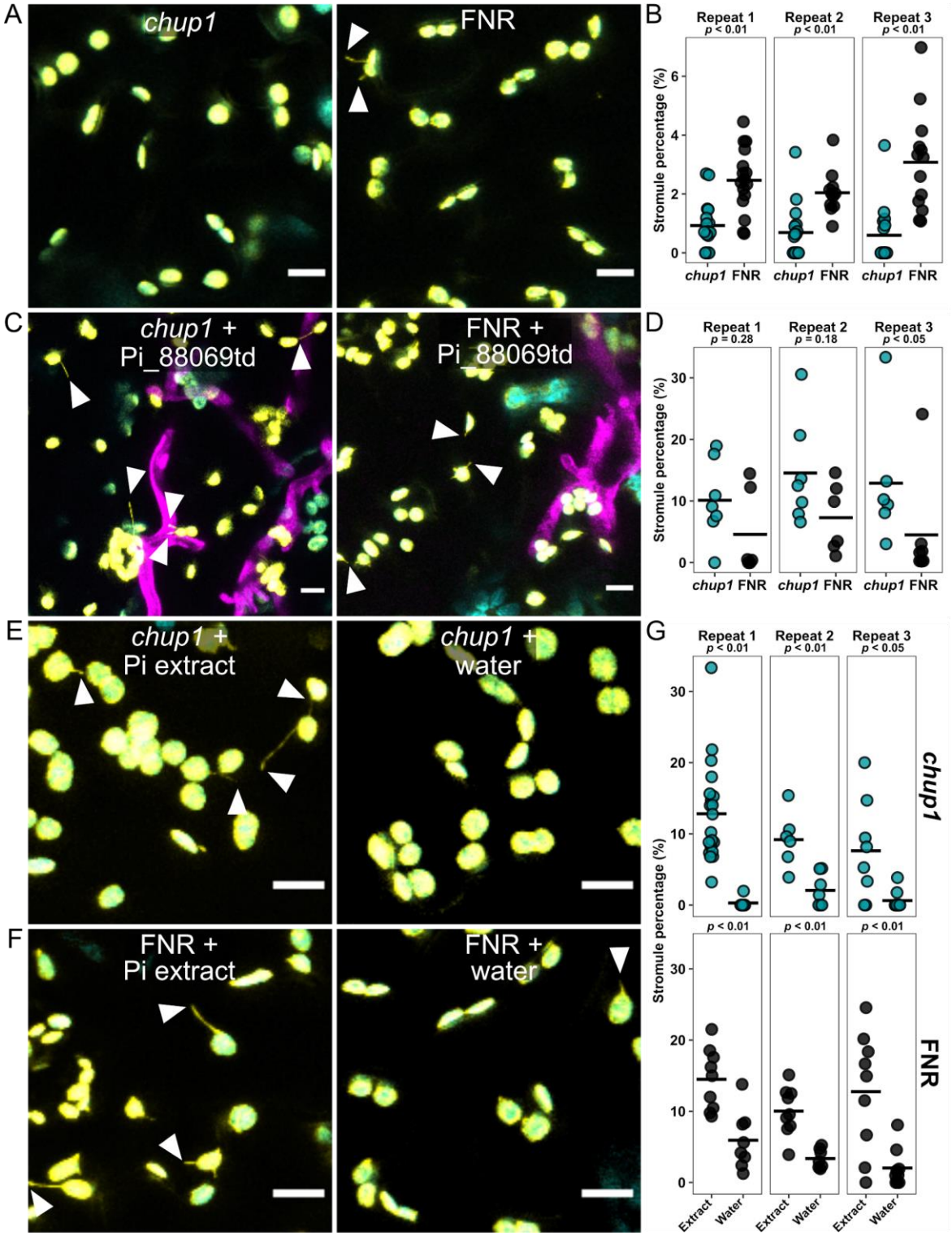

Figure 3: *Chup1* is required for basal stromules but not for immune induced stromules. Throughout all confocal micrographs (A, C, E, F), cyan shows chloroplast autofluorescence, yellow shows stroma targeted GFP, magenta shows *P. infestans* 88069td, arrowheads mark stromules, scale bars are 10 µm. For scatter plots throughout (B, D, G), each data point represents one quantified image, cross bar represents group mean, *p*-value calculated from Wilcoxon test. (A) Maximum projection confocal micrographs *N. benthamiana* epidermal cells of untreated *chup1* and FNR across three separate plants per genotype. (B) Quantification of stromule percentage in untreated *chup1* and FNR plants across three separate plants. (C)

Maximum projection confocal micrographs of *N. benthamiana* epidermal cells during live infection by *P. infestans* 88069td, three days post inoculation, in *chup1* and FNR plants. (D) Quantification of stromule percentage in *chup1* and FNR plants infected by *P. infestans* 88069td (three days post inoculation), across three independent infections on three separate plants per genotype. Stromule data was collected from the same set of micrographs shown and used in Figure 2 to assess chloroplast-haustoria association. (E-F) Maximum projection confocal micrographs *N. benthamiana* epidermal cells following 24 hour treatment with Pi extract or water, in: (E) *chup1* plants; (F) FNR control plants. (G) Quantification of stromule percentage in *chup1* and FNR plants treated with Pi extract or water across three separate plants per genotype.

Chloroplasts show constitutive perinuclear clustering in *chup1* knock-outs

Chloroplasts cluster around the nucleus following a diverse range of immune stimuli, implying that this response (perinuclear chloroplast clustering) may contribute to immunity (Ding et al., 2019). We therefore reasoned that enhanced susceptibility of *chup1* plants could be due to impaired perinuclear clustering of chloroplasts. However, during our imaging of *chup1* plants, we noticed extreme clustering of chloroplasts around what was presumed to be the cell nucleus (Fig. 4A). We validated this observation by transiently expressing a nuclear localized BFP construct (NLS-BFP) via *Agrobacterium tumefaciens* in *chup1* and FNR control plants, which clearly revealed the chloroplasts were clustering around the nucleus in *chup1* plants (Fig. 4B). The extremity of the clustering made manual and automated counting of chloroplasts difficult due to the inability to resolve individual chloroplasts. Instead, the volume of plastid autofluorescence surrounding nuclei was measured to show quantitatively that *chup1* plants had greater perinuclear chloroplast clustering than FNR control plants (Fig. 4C); we validated this method by showing a quantitative increase in the volume of plastid autofluorescence surrounding nuclei in response to a quantitative increase in *A. tumefaciens* GV3101 optical density of infiltration (Fig. S5), as the ability of *A. tumefaciens* GV3101 to induce chloroplast clustering at the nucleus through secreted cytokinin has been reported previously (Erickson et al., 2014). Similarly to the *N. benthamiana chup1* plants, *A. thaliana chup1*-pn lines showed greater perinuclear chloroplast clustering compared to the WT-pn control lines (Fig. S4C).

Given that perinuclear chloroplast clustering has been described as a general response to immune stimulation (Ding et al., 2019), we next set out to determine if this was true for *P. infestans* infections, and if loss of *chup1* affects this response. During infection by *P. infestans* 88069td, both *chup1* and FNR plants responded to infection with an increase in perinuclear clustering of chloroplasts (Fig. S6), but *chup1* plants still displayed significantly greater levels of perinuclear chloroplast clustering compared to the FNR control plants (Fig. S6). Thus, although *chup1* plants have increased perinuclear clustering, they are intriguingly more susceptible to infection; these results suggest that while perinuclear clustering of chloroplasts may be a general response to pathogens and immune stimulation (Ding et al., 2019), it does not necessarily mean increased clustering leads to more immunity.

Multiple studies revealed that the plant nucleus can mobilize and position around the haustorium of fungal and oomycete pathogens during infection (Caillaud et al., 2012; Daniel & Guest, 2005; Freytag et al., 1994; Guest, 1986; Heath et al., 1997; Savage et al., 2021; Schmelzer, 2002). In addition, because chloroplasts are implicated in the movement of nuclei as a response to blue light exposure (Higa et al., 2014; Suetsugu et al., 2016) and they show extreme perinuclear clustering in the absence of *CHUP1* (Fig. 4A-C), we examined whether nucleus localization towards haustoria was at all affected in *chup1* plants. *P. infestans* can penetrate a single host cell with multiple haustoria. Therefore, instead of measuring the

frequency of total haustoria associated with nuclei, we assessed whether the nucleus of a haustoriated cell was associated with a haustorium or not. We did not find any significant difference between *chup1* and FNR plants in nucleus-haustoria association (Fig. 4D-F). Therefore, nucleus-haustoria association during infection is not influenced by the extent of perinuclear chloroplast clustering, nor the absence of *CHUP1*. Taken together, these results indicate that the enhanced susceptibility of *chup1* plants is not due to impaired movement of nuclei to haustoria.

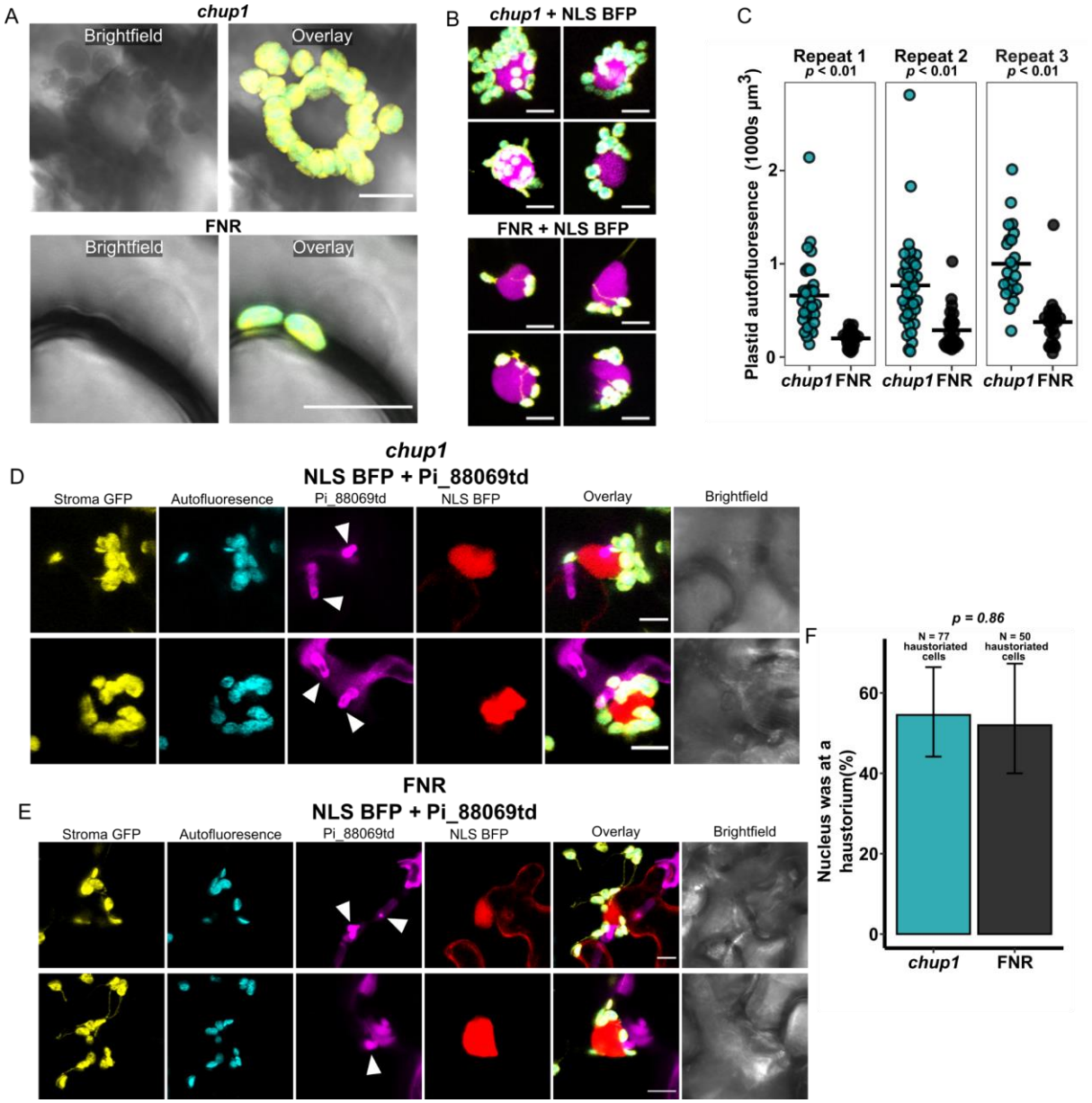

Figure 4: Chloroplasts in the *chup1* plants are greatly clustered around the nucleus, but this does not affect the localization of the nucleus towards haustoria. (A) Maximum projection confocal micrographs of a nucleus in untreated *chup1* (top) and FNR (bottom) plants in epidermal cells. Cyan shows chloroplast autofluorescence, yellow shows stroma targeted GFP. Scale bars are 10 µm. (B) Maximum projection confocal micrographs of nuclei in *chup1* (top) and FNR (bottom) plants transiently expressing NLS-BFP (magenta). Cyan shows chloroplast autofluorescence, yellow shows stroma targeted GFP. Scale bars are 10 µm. (C)

Automated quantifications of chloroplast autofluorescence volume (microns cubed) surrounding nuclei marked by transiently expressed NLS-BFP in *chup1* and FNR plants across three separate plants and agroinfiltrations. Cross bar represents group mean, *p*-value calculated from Wilcoxon test. Each data point represents measurement from a single isolated nucleus. (D-E) Maximum projection confocal micrographs *N. benthamiana* epidermal cells expressing NLS-BFP (red) during live infection by *P. infestans* 88069td (magenta), three days post inoculation, showing representative instances of nucleus-haustoria association in: (D) *chup1* plants; (E) FNR control plants. Cyan shows chloroplast autofluorescence, yellow shows stroma targeted GFP. Intracellular haustoria marked by white arrowheads. Scale bars are 10 µm. (F) Quantified instances of nucleus-haustoria association (as a percentage of total nuclei of haustoriated cells, *N* = 77 and 50 cells in *chup1* and FNR plants respectively). Error bars show 95% confidence intervals, *p*-value calculated from Fisher's Exact test.

CHUP1 is required for Callose deposition at haustorium penetration sites

Next, we explored whether plant immune responses are altered in *chup1* plants. Because focal callose deposition occurs at the site of haustorial penetration during the immune response to pathogen invasion (Bozkurt et al., 2020), we investigated whether this process is perturbed in the absence of *CHUP1*. We used aniline blue staining to visualize and image callose deposition during live infection of *chup1* and FNR plants with *P. infestans* strain 88069td (3 dpi) (Fig. 5A-B). Consistent with our earlier report on callose deposition at *P. infestans* haustoria using the same methodology (Bozkurt et al., 2014), we found around 20% of haustoria in infected FNR plants had focal callose deposits (Fig. 5C); remarkably, *chup1* plants showed callose deposition at only 11% of haustoria (Fig. 5C). These results show *CHUP1* is required for focal callose deposition at the haustoria of *P. infestans*.

Of note, callose deposition did not correlate with the presence of chloroplasts at a haustorium Fig. 5A-B; quantifying this in the FNR plants, we found that of the 29 haustoria where callose was deposited, 13 were chloroplast associated (44.8%) and 16 were not chloroplast associated (55.2%), approximately reflecting the proportions of all haustoria that are chloroplast associated/unassociated in other experiments (Fig. 2C). This reveals that focal callose deposition does not exclusively coincide with the presence of chloroplast at haustoria. However, our experiments are reflective of a snapshot in time during intracellular infection, and therefore without continuous time lapse imaging, we cannot exclude the possibility that focal callose deposition requires chloroplast mobilization towards haustoria, as chloroplast may have moved away from haustoria at the time of imaging.

We then investigated whether other core immune pathways were perturbed in the *chup1* plants. To determine whether immune responses following PAMP recognition are altered in the absence of *CHUP1*, we tested for the mitogen-activated kinase (MAPK) phosphorylation following infiltration of leaves with Pi extract. Both *chup1* and FNR control plants showed a comparable increase in MAPK phosphorylation 24 hours after infiltration of Pi extract relative to infiltration with water control (Fig. 5D). We then tested whether late-stage immune responses such as defense related cell death activation was impaired in the *chup1* plants. Following transient *Agrobacterium* expression of an auto-active variant of a MEK2-like NbMAPKK tagged to 3xHA ($MEK2^{DD}$ 3xHA) (Yang et al., 2001), both *chup1* and FNR plants produced a strong cell death phenotype compared to the Luciferase 3xHA control (Fig. 5E & S6). Both *chup1* and FNR plants had similar levels of *Agrobacterium* mediated transient expression of Luciferase 3xHA and $MEK2^{DD}$ 3xHA, although protein extraction from areas with extreme cell death was very challenging to normalize, as is reflected in loading controls (Fig. S7).

To test whether effector triggered immunity is perturbed in the absence of *CHUP1*, we co-expressed *P. infestans* RXLR effector AVR3a with its cognate NLR receptor R3a (Bos et al., 2009). This revealed that both *chup1* and FNR plants can induce cell death to similar degrees (Fig. 5F & S7), whereas we did not observe any cell death when AVR3a and R3a were infiltrated alone as additional controls (Fig. S8). All together, these results demonstrate that activation of PAMP or effector triggered immunity are not impaired in the absence of *CHUP1*, and enhanced susceptibility of *chup1* plants is most likely due to reduced focal deployment of callose at the haustorium interface.

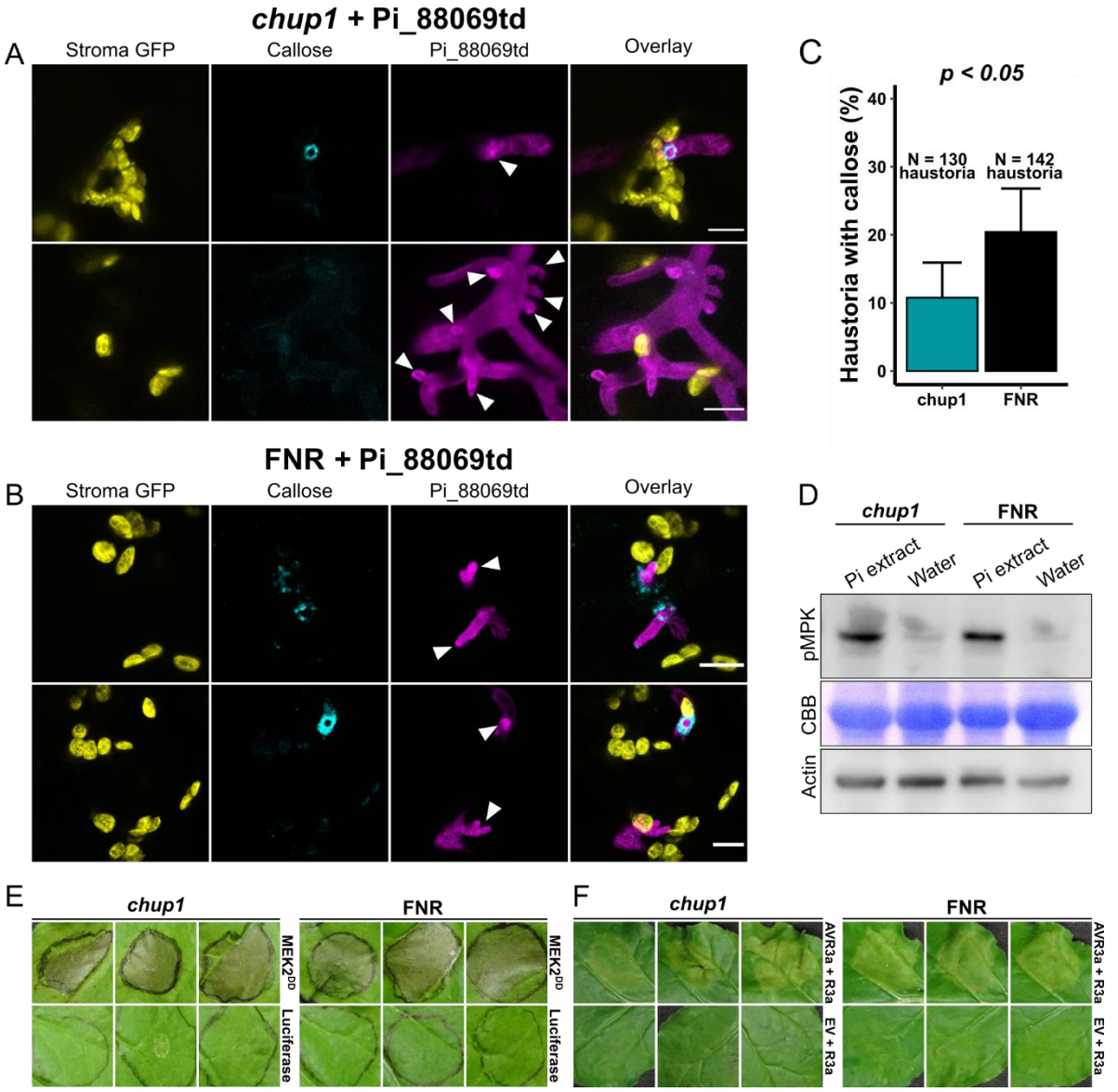

Figure 5: *CHUP1* is required for proper deposition of callose at haustoria. (A-B) Maximum projection confocal micrographs *N. benthamiana* epidermal cells during live infection by *P. infestans* 88069td (magenta), three days post inoculation, following a 2 hr aniline blue stain, showing representative instances of callose deposition haustoria association in: (A) *chup1* plants; (B) FNR control plants. Cyan shows callose deposition, yellow shows stroma targeted GFP. Intracellular haustoria marked by white arrowheads. Scale bars are 10 µm. (C) Quantified instances of callose deposition at haustoria (as a percentage of total haustoria, *N* = 130 and *N* = 142 haustoria in *chup1* and FNR plants respectively). Error bars

show 95% confidence intervals, *p*-value calculated from Fisher's Exact test. (D) Western blot detection of phosphorylated MAPKs in *chup1* and FNR plants following 24 hour treatment with either Pi extract or water. CBB = coomassie brilliant blue staining of gel post transfer of proteins and actin detection shown for loading controls. (E) Cell death assay following transient expression of $MEK2^{DD}$ 3xHA or Luciferase (Luc) 3xHA control. Photographs of infiltrated tissue were taken three days post infiltration. Three representative images of each condition shown (all infiltrations from experiment shown in (Fig. S7). (F) Cell death assay following transient co-expression of R3a with AVR3a or empty vector control. Photographs of infiltrated tissue were taken three days post infiltration. Three representative images of each condition shown (all infiltrations and additional controls from experiment shown in (Fig. S8).

Discussion:

We recently showed that chloroplasts accumulate around *P. infestans* haustoria and intimately associate with the EHM (Savage et al., 2021). Here, we investigated whether chloroplast movement and positioning contribute to plant focal immune responses. We discovered that CHUP1, the chloroplast outer envelope protein that mediates light dependent chloroplast movement and membrane attachment, is required for basal resistance to *Phytophthora infestans* (Fig. 1). Loss of *CHUP1* did not alter chloroplast positioning around the haustorium (Fig. 2) but did enhance chloroplast gathering around the nucleus (Fig. 4), a process that typically occurs upon pathogen or PAMP recognition. While loss of *CHUP1* reduced the stromule frequency under normal conditions, it did not dampen the induction of stromules in response to immune stimulation (Fig. 3), indicating that enhanced susceptibility phenotype in *chup1* knock-outs is not caused by impaired stromule induction during infection. Finally, we show that *CHUP1* is required for proper deposition of callose towards haustoria, yet not for other core immune processes such as MAPK triggered signaling and cell death as well as effector triggered HR (Fig. 5). We conclude that *CHUP1* contributes to plant focal immunity by facilitating callose deposition at the pathogen penetration sites. Our results support a role of *CHUP1* in pathogen penetration resistance through cell wall reinforcement at the pathogen contact sites.

Chloroplasts contribute to focal immunity by facilitating callose deposition at the pathogen interface

One of the hallmarks of cell polarization during pathogen attack is the focal deployment of callose at the pathogen contact sites, a general plant immune response deployed to counteract pathogen penetration (Ellinger et al., 2013). Unlike haustoria of obligate biotrophic oomycetes and fungi (Caillaud et al., 2014; Micali et al., 2011), *P. infestans* haustoria are typically only partially encased by a 'collar' of callose deposited around the neck of around 20% of haustoria (Bozkurt et al., 2014). Here we found that *CHUP1* is required for consistent deployment of callose at the haustorium interface, as cells lacking *CHUP1* had a 50% reduction in the number of *P. infestans* haustoria that show callose staining (Fig. 5). Like CHUP1, chloroplast-localized proteins NHR2A and NHR2B were reported to contribute to non-host resistance to a bacterial pathogen and callose deposition following immune activation (Singh et al., 2018). Intriguingly, both CHUP1 and NHR2A/B localize to the chloroplast periphery, hinting at a potential co-operative role of these proteins to facilitate callose accumulation at the plant-pathogen interfaces, an exciting avenue for future research. In agreement with these findings, a more recent study revealed that CHUP1 is required for non-host penetration resistance during fungal infection of Arabidopsis (Irieda & Takano, 2021). Combined with these reports, our findings that a chloroplast protein contributes to resistance to an adapted pathogen and proper deposition of callose at haustorium penetration sites

reveal that chloroplasts play an active role in plant focal immunity against both adapted and non-adapted pathogens.

What is the link between chloroplasts and callose?

But what role does a chloroplast outer envelope protein play in the focal deployment of callose around the haustorium? Chloroplasts produce several molecules that have been implicated in callose deposition, including reactive oxygen species (ROS) (Shapiguzov et al., 2012) and precursors of the defense hormones such as salicylic acid (Serrano et al. 2016). Therefore, a reduction in the production of these molecules, and/or the regulation of their release from the chloroplasts, could plausibly be responsible for impaired callose accumulation at the haustorium interface.

Compared to other subcellular compartments, photosynthesizing chloroplasts generate large amounts of ROS via electron transfer reactions (Asada, 2006; Foyer & Noctor, 2003). Chloroplast ROS contributes to antibacterial immunity (Zurbriggen et al., 2009), whereas pathogenic bacteria deploy effectors to disrupt ROS generated through photosynthetic machinery (Rodríguez-Herva et al., 2012). ROS is required for cell wall fortification through crosslinking of cell wall proteins and phenolics, as well as callose deposition (Brown et al., 1998; Daudi et al., 2012; O'brien et al., 2012; Thordal-Christensen et al., 1997). Activation of plant immunity stimulates MAPK signaling cascades that rapidly down-regulate photosynthetic gene expression and upregulates ROS accumulation in chloroplasts (Su et al., 2018). Unfortunately, we were not able to measure the redox state of *chup1* chloroplasts, because the transgenic *chup1* plants carried a chloroplast localized GFP (to enable monitoring of stromules) which has an overlapping emission spectra with the HyPer ROS sensor (Belousov et al., 2006) that we previously used to observe elevated chloroplast ROS during *P. infestans* infection live cell imaging (Savage et al., 2021). Since internal ROS production stimulates stromule formation (Brunkard et al., 2015), it is possible that perturbations in the redox state of chloroplasts could be responsible for impaired callose accumulation and enhanced induction of stromules in infected *chup1* plants. Consistent with this, *chup1* plants had higher rates of stromule induction upon pathogen challenge, despite having reduced basal levels of stromules (Fig. 3A-D), possibly due to greater accumulation of chloroplastic ROS. This hypothesis would imply a role for *CHUP1* in chloroplast ROS production, accumulation, and/or release during infection that stands to be investigated in the future.

Alternatively, a perturbation in chloroplast derived salicylic acid (SA) levels could also plausibly affect callose deposition, as SA has been previously linked to callose deposition at plasmodesmata during immune challenge (X. Wang et al., 2013). Additionally, SA application has been shown to induce stromules in *N. benthamiana*, which could also explain the stromule phenotypes of the *chup1* plants (Caplan et al., 2015). However, given we did not see differences in cell death (which is differentially regulated by SA) between the *chup1* and FNR plants, SA may be a less likely candidate to explain the callose phenotype (Radojičić et al., 2018).

Perinuclear chloroplast clustering and immunity

The perinuclear clustering of chloroplasts has been reported in a range of plants and tissue types (Kwok & Hanson, 2004; Sheahan et al., 2004, 2020). This response has been described in the context of cell division (Sheahan et al., 2020), and more recently, of immunity (Caplan et al., 2015; Ding et al., 2019; Kumar et al., 2018). Caplan et. al. (2015) described an increase in stromule-to-nucleus connection during activation of the hypersensitive response by viral p50 protein in *N. benthamiana*. Following on from this, Ding et. al. (2019) showed the induction of perinuclear chloroplast clustering following activation of diverse immune pathways. Taken

together, these studies strongly suggest an immune function of chloroplast-nucleus association; our results also show live *P. infestans* infection induces the aggregation of chloroplasts at the nucleus (Fig. S6), supporting the hypothesis. However, we show that despite more extreme perinuclear clustering in *chup1* plants (Fig. 4), susceptibility to *P. infestans* is increased (Fig. 1). This implies that a higher degree of chloroplast-nucleus contact does not necessarily provide greater immunity; indeed, extreme (with regards to severity) and mis-regulated (with regards to timing) clustering may in fact impair a proper immune response. Further research is needed to determine the extent to which perinuclear chloroplast accumulation contributes to immunity.

Perturbations in stromule frequency in *chup1* knock-outs

Our data reveal that loss of *CHUP1* leads to reduced basal stromule levels, but somehow enhances the rate of stromule induction during infection by *P. infestans* (Fig. 3). Because *CHUP1* mediates actin dependent chloroplast movement, the reduced stromule frequency under normal conditions could be explained by decreased chloroplast motility. On the other hand, enhanced induction of stromules upon pathogen challenge could be due to altered redox state of chloroplasts in *CHUP1* mutants as we outlined earlier. *CHUP1* has previously been implicated in the production of stromules, where Caplan et. al. (2015) reported a constitutive induction of stromules during virus induced gene silencing (VIGS) of *CHUP1* in *N. benthamiana* and in *chup1* knock-out lines of *A. thaliana*. Our data conflict with those of Caplan et. al. (2015) as we did not find any increased stromule frequency in Arabidopsis and *N. benthamiana chup1* knock-outs. This discrepancy in *N. benthamiana* could be due to different approaches used to deplete *CHUP1*; whereas our *N. benthamiana* data is based on CRISPR mediated *CHUP1* knock-outs, Caplan et al. (2015) used TRV based VIGS to knock-down *CHUP1*. Interestingly, our data shows an enhanced stromule induction in *chup1* knock-outs during infection. Therefore, the presence of TRV in VIGS assays conducted by Caplan et al. (2015) could be responsible for enhanced stromule frequency upon *CHUP1* silencing. However, the discrepancy of stromule frequency in Arabidopsis mutants observed by Caplan et al. (2015) and us could be due to different chloroplast marker proteins used; NRIP1-GFP and GFP localized to stroma, respectively. The NRIP1 marker used by Caplan et al. (2015) is implicated in plant immunity and could potentially alter stromule frequency when overexpressed.

The last decade have unearthed prominent roles of organelle membrane contact sites in intracellular signaling and cellular stress responses (Prinz et al., 2019). Accumulating evidence suggests organelles such as chloroplasts and mitochondria contribute to plant immunity and position themselves at the pathogen interface (Fuchs et al., 2016; Savage et al., 2021). An intriguing link between mitochondria and fungal penetration resistance have been found, revealing that mitochondria accumulate at fungal invasion sites (Fuchs et al., 2016). Notably, these mitochondria accommodated atypical myrosinase PENETRATION2 (PEN2) that is required for penetration resistance (Fuchs et al., 2016), suggesting that mitochondria could contribute to plant focal immunity. Here, we revealed that chloroplast movement and membrane attachment protein CHUP1 is required for focal deployment of callose at the pathogen interface, highlighting that chloroplast play an active role in plant focal immune responses. Further research is required to determine the extent to and mechanism by which *CHUP1* facilitates proper callose deposition at the haustorium interface and contributes to penetration resistance. Understanding the means by which chloroplasts and other organelles communicate with each other to prevent pathogen invasion remains as an interesting future research direction.

Materials & Methods:

Plant materials

Nicotiana benthamiana plants were grown at 25°C under high light intensity for 16 hr day, 8 hr dark light cycling for 4-5 weeks before use in experiments.

Two different transgenic *N. benthamiana* expressing plastid localized eGFP, referred to as CpGFP (Savage et al., 2021) and FNR (Erickson et al., 2014), were used in experiments. FNR was the parental line for the *chup1* knock-out plants and was used as a control for all *chup1* related experiments. A double marker line of *N. benthamiana* expressing plastid localized eGFP and nuclear localized mCherry was also used (Erickson et al., 2017).

Generation of *Nbchup1* lines

The following primer pairs were used for the generation of guide RNA sequences that target both *NbChup1* alleles:

attGCAAGATCAAGGAGTTGCAG & aaacCTGCAACTCCTTGATCTTG;
attgTGGACTTCAAGAAAAGGAAG & aaacCTTCCTTTTCTTGAAGTCCA;
attgTCTGTATCATACTTGTCACT & aaacAGTGACAAGTATGATACAGA

The recipient genome editing vector was: pDGE463 (Stuttmann et al., 2021);. pDGE463 harbors: plant kanamycin resistance (positive selection of transgene); Bs3 gene from pepper (negative selection of transgene); 2xtagRFP expressed by a seed coat specific promotor (negative selection of transgene); p35S driven intronized Cas9 2xNLS; bacterial spectinomycin resistance. The recipient genome editing vector containing the guide RNAs was called pDGE472.

The parental line transformed was NbFNR:eGFP_7-25 (FNR) (Schattat et al., 2011). This parental line was then used as a control line throughout the manuscript.

Arabidopsis thaliana

Arabidopsis thaliana plants were grown at 21°C for 16 hr day, 8 hr dark light cycling for 4-6 weeks before use in experiments. The *A. thaliana* T-DNA insertion line SALK_129128 that results in a knock-out of *CHUP1* was used. For visualization of plastids and nuclei, this line was transformed with plsu4pn by standard floral dipping procedure (Davis et al., 2009). Plsu4pn is composed of a p35S:FNR:eGFP:t35S and pAtUBQ10:H2B:mCherry:tNOS (Erickson et al., 2017). Transgenic *A. thaliana* expressing plastid localized eGFP and nuclear localized mCherry (WT-pn) were also used as a control line (Erickson et al., 2017).

Phytophthora infestans inoculation

Transgenic *Phytophthora infestans* strain 88069td expressing tdTomato fluorescence protein was cultured on rye sucrose agar (RSA) plates for 12-16 days at 18°C in the dark (Whisson et al., 2007).

For infection assays and live infection microscopy, zoospores were harvested from plates of *Phytophthora infestans* 88069td by addition of 4-5 mL of 4°C glass distilled water and incubation of soaked plates for 2 hr. Residual liquid containing released zoospores was collected and adjusted to contain approximately 50,000 spores per mL after counting initial spore concentration using a haemocytometer. 10 µL droplets of spore solution were pipetted onto the abaxial side of detached leaves. Infected leaves were kept at 18°C (16 hr day, 8 hr dark light cycling) in a sealed, clear plastic box kept humid with moist paper towels. For live

infection microscopy, infections were left for 3-4 days, for infection assays, infections were left for 4-5 days.

Infection assays

Images of hyphal growth were captured on a Leica DFC300 FX fluorescent microscope (Leica Microsystems, Germany) using the DSR UV filter. For six infection droplets on a single leaf, the mean hyphal growth from the six was taken and used as a single data point for analysis. Hyphal growth was measured using ImageJ (Schneider et al., 2012) via a custom macro that, in brief, converts images to 8-bit, auto-thresholds (method = "Huang"), and measures the total area limited to the threshold region. The proportion of this area relative to that of the total image field of view (100*(threshold area/total area)) was used as the measure of infection for each infection.

Western blotting

Protein extraction, SDS-PAGE, and Western blotting was performed as described previously (Bozkurt et al., 2011). Polyclonal rabbit anti-phosphorylated MAPK (Phospho-p44/42 MAPK, Cell Signaling Technology), and monoclonal rat anti-HA (7C9, Chromotek) were used as primary antibodies; anti-rabbit peroxidase (Sigma-Aldrich, UK), and anti-rat alkaline phosphatase (Sigma-Aldrich) antibodies were used as secondary.

Phytophthora infestans extract treatment

To harvest an extract from RSA plates of *Phytophthora infestans* by removing the hyphae layer that grows on the plate using a scalpel and resuspending this in 5 mL of autoclaved dH_2O. The suspension was boiled at 90°C for 10 minutes and then filtered through miracloth. The filtrate was centrifuged for 30 min at maximum speed at 4°C. The supernatant was passed through a 0.45 µm syringe filter. Extract was stored at -20°C.

Agrobacterium mediated expression

Agrobacterium tumefaciens strain GV3101 was used throughout (Hellens et al., 2000) for transient expression in 3-4 week old *Nicotiana benthamiana* as previously described (Bozkurt et al., 2011). *A. tumefaciens* cultures were grown over two days and resuspended in 1 mL of water for washing. The suspension was centrifuged at 1500 *g* and the supernatant removed before a second wash was completed. After the second wash, the bacteria was resuspended in agroinfiltration buffer (10 mM 2-(N-morpholino-ethanesulfonic acid hydrate (MES hydrate), 10 mM MgCl2, pH 5.7). The OD_{600} was adjusted depending on the construct being expressed and the experiment in question. For $MEK2^{DD}$ 3xHA, OD_{600} = 0.1; AVR3a, R3a, EV pICSL86977, OD_{600} = 0.3; NLS-BFP, OD_{600} = 0.05 (for experiments involving *P. infestans* infection) or 0.1 (for uninfected tissue) unless explicitly stated otherwise; CHUP1 3xHA, OD_{600} = 0.3; Luciferase 3xHA was used as a control and matched in OD_{600} to construct used for the experimental condition.

Confocal microscopy

Leaf tissue was prepared by cutting a leaf disk and mounting in wells made of Carolina Observation Gel that contained water to fully submerge the sample. The abaxial side of the leaf was imaged to focus on epidermal cells, guard and mesophyll cells were avoided when imaging, but this was not always possible. All confocal microscopy was completed using a Leica SP8 resonant inverted confocal microscope (Leica Microsystems) using a 40X objective 1.2NA Plan-Apochromat water immersion objective. Specific excitation wavelengths and filters for emission spectra were set as described previously (Koh et al., 2005). GFP emission was detected at 495-500 nm following excitation by 488 nm Argon laser; tdTomato emission was

detected at 570-620 nm following excitation by 543 nm excitation by Helium-Neon laser; BFP emission was detected at 410-490 nm following excitation by 405 nm Diode laser.

Confocal image analysis

For all manual counts from confocal micrographs, image names were randomized to blind the experimental condition from the rater (https://imagej.nih.gov/ij/macros/Filename_Randomizer.txt ; Tiego Ferreira, 2009); this was to reduce potential bias in final quantifications.

Automated plastid counting

Plastids were automatically counted using a custom ImageJ script. Briefly, maximum intensity z-projections of z-stack images were made, and channels split. The autofluorescence channel was automatically thresholded (method = “Li”), a watershed applied, and objects counted by the “Analyze particles” command (size = 5-35). Stromules for the same set of images were manually counted from the GFP stroma channel.

Chloroplast-haustoria association

Association between chloroplasts and haustoria was counted manually. First, haustoria were identified in a given z-stack from using only the *P. infestans* 88068td and brightfield channels - this avoided haustoria identification being influenced by the position of chloroplast. Next, the number of those haustoria associated with a chloroplast was counted, including if the chloroplast was contacting the haustoria via a stromule. Percentage of haustoria associated with chloroplasts was calculated based on the total number of haustoria identified. This percentage of the entire data set was used instead of calculating image-by-image percentage association to avoid data being skewed by images containing a single haustorium giving a 0 or 100% readout for association.

Perinuclear clustering

The extremity of perinuclear chloroplast clustering made resolution of individual chloroplasts challenging. Perinuclear clustering was measured as the total voxels of thresholded chlorophyll autofluorescence in the vicinity of automatically identified nuclei. First, nuclei were automatically identified. Maximum intensity z-projections of z-stack images were made, and channels split. The NLS-BFP (or NLS mCherry) channel was automatically thresholded (method = “Li”), a watershed applied, and objects counted by the “Analyze particles” command (size = 100-500). The position of the identified object was saved as a region of interest (ROI). For each ROI position, the original image was duplicated and cropped (70x70) to produce an image containing only the isolated nucleus; these were saved separately for the next step. The quality of identified crops was then assessed manually, and only if necessary, the following adjustments were made: a) slices of the z-stack removed that contained the mesophyll layer, b) cropped again smaller to exclude chloroplasts that were in an adjacent cell or not in immediate contact with the isolated nucleus. Finally, the plastid autofluorescence in the vicinity of the nucleus was measured (as a metric for perinuclear clustering) as follows. Briefly, chloroplast autofluorescence channel was isolated, automatically thresholded (method = “Li”), next pixels with a value 255 were counted for each slice of the z-stack and the voxel size identified for each image to give a custom table containing pixel count, voxel size, and image name for all identified nuclei. With this the cubic microns of thresholded chloroplast autofluorescence could be calculated for each identified nucleus.

To validate our method, we induced perinuclear chloroplast clustering by using the *A. tumefaciens* GV3101 strain as a positive control which secretes cytokinin that triggers this

process (Erickson et al., 2014). Infiltration of different optical densities of *A. tumefaciens* GV3101 to transgenic *N. benthamiana* expressing nuclear localized mCherry led to a greater perinuclear chloroplast clustering in cells infiltrated with higher optical densities of *A. tumefaciens* GV3101 (Fig. S5).

Nucleus-haustoria association

Cells were identified from z-stacks that were both haustoriated and had the nucleus visible within the z-stack; only cells fulfilling these criteria were considered. For each of these cells, the nucleus was categorized as either: a) associated with a haustoria, b) distant from a haustoria (i.e. not associated). This system was used instead of looking at the percentage of total haustoria associated as many cells contain multiple haustoria, and therefore, despite localization of the nucleus towards haustoria, haustoria-nucleus association may appear low. The total percentage of nuclei associated with a haustoria was then calculated based on the total nuclei in haustoriated cells counted across the entire data set.

Epi-fluorescent imaging of *A. thaliana*

For image acquisition, an epi-fluorescence microscope (AxioObserver Z1) setup from Zeiss (Jena, Germany) equipped with an X-Cite fluorescence light source and a MRm monochrome camera (Zeiss, Jena, Germany) was used. GFP fluorescence was recorded using a 38 HE filter cube (Carl Zeiss AG, Jena, Germany). mCHERRY fluorescence was recorded utilizing the 43 HE filter cube (Carl Zeiss AG. Jena, Germany). The microscope manufacturers software (ZenBlue, Zeiss, Germany) controlled image acquisition. All images were captured using a 40x / 0.75 NA EC PLAN NEOFLUAR lens.

For quantification of stromule frequencies, a single square of a fully expanded leaf from a 4 to 6 week old plant was harvested. Samples were vacuum-infiltrated, mounted on glass slides and three independent z-stacks of the lower epidermis were collected in transmitted light, eGFP and mCHERRY channels. In order to obtain 2D extended depth of field images for quantification, single images of the z-series of each channel were first exported into separate file folders and subsequently combined into single images using software and procedures described in Klösgen & Schattat (2009) (total of 3 images per disc).

Statistical analysis

Analysis of infection assays, stromule percentages, and perinuclear clustering were analyzed using a t test when groups were normally distributed (as determined by Shapiro-Wilk test) and a Wilcoxon test when groups were not normally distributed. Here, biological replicates (samples from separate plants), were analyzed independently and presented as such in figures. Quantification of haustoria-chloroplast association, nucleus-haustoria association, and callose deposition at haustoria were pooled together from the entire data set to generate an overall proportion/percentage from all micrographs; this was done to avoid data skew by micrographs that contained only one haustoria and would therefore generate many 100% and 0% values that skew the mean estimate. The proportions of each observation were compared using a Fisher's Exact test. All analyses were conducted using R.

Molecular cloning and plasmid constructs

The NLS-BFP construct was made by joining a cut C-terminal BFP vector with a single stranded DNA oligo bridge via Gibson assembly. The single stranded DNA oligo bridge (Eurofins) had overhangs for the cut vector ends that flank the coding sequence for the SV40 nuclear localization sequence (PKKKRKVEDP, (Goldfarb et al., 1986)). The DNA oligo bridge nucleotide sequence was:

GGCGGCCGCACTAGTGATGCCTAAAAAGAAGCGTAAGGTTGAGGACCCTGATATCGGA
TCTGCTGGATCT.

The VIGS CHUP1 construct, was constructed by amplifying a region of the *CHUP1* sequence from *N. benthamiana* cDNA using the primer pair:
AGAATGAAATGGTTGCCC & GATCCTGCGTATTCTAACATC. The amplified fragment was then cloned into a Gateway compatible pTRV2 vector using Gateway Technology (Invitrogen).

Full length Luciferase coding sequence was PCR amplified from the pGEM-luc cassette vector (Promega) using the primer pair:
CAGGCGGCCGCACTAGTGATGGAAGACGCCAAAAACATAAAG &
GCAGATCCAGCAGATCCGATCAATTTGGACTTTCCGCCC. The PCR product was then inserted into a cut C-terminal 3xHA vector.

CHUP1 3xHA was generated by amplifying two PCR products (Phusion DNA polymerase, Thermo Scientific) from *N. benthamiana* cDNA, amplifying CHUP1-a (herein CHUP1) using two different primer pairs (AGGCGGCCGCACTAGTATGATAGTCAGGGTAGGTTTAGTG
G & GTTCCAAAACTAGTGATGGCTAC; GCTCAGAAATGCAGGTGATGGT &
TCCTCGCCCTTGCTCACCATTGATCCTGTTTCTTGTGTATTC
TCTTCTCC) to generate two PCR products with complementary overhangs to each other and the 3xHA C-terminal vector. The PCR products were assembled and cloned into a cut C-terminal 3xHA vector.

The full coding sequence for MEK2^{DD} was synthesized by Genewiz with complementary overhangs to the 3xHA C-terminal vector, allowing for Gibson Assembly of the synthesized fragment into the vector. The gene sequence synthesized was the following:

CAGGCGGCCGCACTAGTGATGCGACCTCTTCAACCACCCCCACCAGCCGCCGCCGCC
ACCACTACCTCCTCTTCCACCACCGCATCACCCATGCCCCCTCCTCCTTCACGCAACCG
TCCCCGTCGTCGTACCAATTTAACTCTCCCCCTTCCCCAACGTGACCCAGCTCTCGCCG
TACCCCTCCCCCTCCCCCCTACTTCCGCCCCTTCTTCCTCGTCGTCTTCCTCTTCCTCC
CCACTCCCCACCCCCTTAAACTTCTCCGAACTTGAGCGCATCAATCGCATCGGCAGCG
GCGCTGGCGGTACGGTTTACAAAGTCCTATATCGCCCCACCGGAAGACTCTACGCTCT
CAAAGTCATCTACGGTAACCACGAGGACTCCGTTCGCCTTCAGATGTGCCGTGAGATC
GAGATTCTCCGTGACGTCGACAACCCTAACGTCGTTAGATGTCACGATATGTTCGATCA
CAACGGTGAAATCCAAGTCCTCCTTGAATTCATGGATAAAGGCTCTCTTGAAGGGATCC
ACATCCCTAAAGAGTCAGCTCTTTCGGATCTAACCCGACAAGTCCTCTCGGGACTCTAT
TATCTCCACAGGCGTAAGATTGTGCACAGAGATATCAAGCCCTCGAATTTACTAATCAA
CTCGAGGCGTGAGGTGAAAATTGCTGACTTTGGGGTGTCGAGAGTGCTGGCACAAGAC
ATGGATCCTTGTAATGATTCAGTTGGGACAATTGCCTATATGAGTCCAGAGAGAATCAA
CACAGATCTGAATCATGGACAGTACGATGGGTATGCTGGAGATATATGGAGTCTTGGTG
TTAGCATATTGGAGTTTTATTTGGGAAGGTTTCCGTTTTCTGTTGGGAGGTCAGGTGATT
GGGCTAGTCTTATGTGCGCCATTTGTATGTCGCAGCCGCCGGAGGCTCCGGCGAATGC
TTCTAGAGAGTTCAGGGACTTTATTGCTTGCTGTTTGCAGAGGGATCCTGCGCGGCGG
TGGACGGCGGTGCAGCTGTTGCGTCATCCATTTATTACCCAGAATAGACCAGCCACTA
CCACCACCGGTAATATGATGCCACTTCCTAATCAAGTTCATCAGCCAGCACATCAATTG
TTACCCCCGCCTCATTTTTCTTCTATCGGATCTGCTGGATCTGC

High fidelity PCR reactions were completed with Phusion DNA polymerase. PCR products were assembled with vectors by Gibson assembly (Gibson et al., 2009). The following were cloned and described previously: AVR3a cloned in pICSL86977 was provided by TSLSynBio;

R3a (Chaparro-Garcia et al., 2015). All C-terminal tagging constructs are derivative of pK7WGF2 as described previously (Duggan et al., 2021), these vectors were all cut using EcoRV.

Cell death assays

Cell death assays were completed via transient *Agrobacterium* mediated expression or by infiltration of *P. infestans* extract as described above. Cell death was visually assessed and photographed 3 days post agroinfiltration (dpi) for MEK2^{DD} 3xHA/Luciferase 3xHA assays and 4 dpi for ARV3a/R3a and *P. infestans* extract/water assays. Instead of using a subjective scale to score the cell death, all data collected (i.e. photographs taken) has been shown in the supplementary figures. To check protein expression levels were even between conditions for the MEK2^{DD} 3xHA/Luciferase 3xHA cell death assays, tissue was collected from the infiltrated regions of each leaf for Western blot analysis. Extracting protein evenly from the dead tissue was challenging due leaf not cutting cleanly.

Chlorophyll extraction

Three leaf disks (No. 4 cork borer) from three different leaves were taken from each plant. Each leaf disk was ground in 10 mL of methanol for 1 minute and spun at 2000 rpm for 5 min. Absorbance at 666 and 653 nm was measured, and total chlorophyll concentration calculated as in Wellburn et. al. (1994).

RT-PCR

60 mg of leaf tissue was excised from 5-week old leaves (VIGS experiments) and frozen in liquid N_2. RNA was extracted from the leaf tissue using the Plant RNA Isolation Mini Kit Protocol (Agilent Technologies). RNA quality and concentration was measured using a NanoDropTM Lite Spectrophotometer (Thermo Scientific). cDNA was synthesized using as a template 2 µg of RNA following the SuperScript II RT protocol (Invitrogen). To amplify the cDNA, a standard PCR (RT-PCR) was then performed using DreamTaq DNA polymerase (5 U/µL) (Thermo Scientific). VIGS-CHUP1 silencing was confirmed by separately amplifying *CHUP1a* and *CHUP1b* from cDNA with the following primer pairs:

ATGATCGTCAGGGTAGGTTTAGTGGTTGC & TGTTTCTTGTGTATTCTCTTCTCCTGTTTGT; TGATAGTCAGGGTAGGTTTAGTGGTTGC & TGTTTCTTGTGTATTCTCTTCTCCTGTTTGA

Virus induced gene silencing (VIGS)

Agrobacterium was prepared as above carrying TRV1 and the appropriate TRV2 construct and mixed to a final OD_{600} of 0.4 or 0.2 respectively, in agroinfiltration buffer supplemented with 100 µM acetosyringone (Sigma) and left in the dark for 2h prior to infiltration to stimulate virulence. 14-day old *N. benthamiana* seedlings were infiltrated in both cotyledons and any true leaves that had emerged. *N. benthamiana* plants were infiltrated with TRV1 and TRV2-CHUP1 for CHUP1-silencing and TRV1 and TRV2-EV for the empty vector control. Plants were left to grow under standard conditions until experiments could be carried out four weeks later.

Acknowledgements:

TOB's lab is funded by the Biotechnology and Biological Sciences Research Council (BBSRC; BB/M002462/1). The Facility for Imaging by Light Microscopy (FILM) at Imperial College London is part supported by funding from the Wellcome Trust (grant 104931/Z/14/Z) and BBSRC (grant BB/L015129/1). MS's lab is funded by the Deutsche Forschungsgemeinschaft (DFG, German Research Foundation) – 400681449/GRK2498 as well as Martin-Luther-University core funding.

References:

Asada, K. (2006). Production and scavenging of reactive oxygen species in chloroplasts and their functions. *Plant Physiology*, *141*(2), 391–396. https://doi.org/10.1104/PP.106.082040

Belousov, V. V., Fradkov, A. F., Lukyanov, K. A., Staroverov, D. B., Shakhbazov, K. S., Terskikh, A. V., & Lukyanov, S. (2006). Genetically encoded fluorescent indicator for intracellular hydrogen peroxide. *Nature Methods*, *3*(4), 281–286. https://doi.org/10.1038/nmeth866

Bos, J. I. B., Chaparro-Garcia, A., Quesada-Ocampo, L. M., Gardener, B. B. M., & Kamoun, S. (2009). Distinct amino acids of the Phytophthora infestans effector AVR3a condition activation of R3a hypersensitivity and suppression of cell death. *Molecular Plant-Microbe Interactions : MPMI*, *22*(3), 269–281. https://doi.org/10.1094/MPMI-22-3-0269

Bozkurt, T. O., Kamoun, S., & Lennon-Duménil, A.-M. (2020). The plant–pathogen haustorial interface at a glance. *Journal of Cell Science*, *133*(5), 133. https://doi.org/10.1242/JCS.237958

Bozkurt, T. O., Richardson, A., Dagdas, Y. F., Mongrand, S., Kamoun, S., & Raffaele, S. (2014). The plant membrane-associated REMORIN1.3 accumulates in discrete perihaustorial domains and enhances susceptibility to phytophthora infestans. *Plant Physiology*, *165*(3), 1005–1018. https://doi.org/10.1104/pp.114.235804

Bozkurt, T. O., Schornack, S., Win, J., Shindo, T., Ilyas, M., Oliva, R., Cano, L. M., Jones, A. M. E., Huitema, E., Van Der Hoorn, R. A. L., & Kamoun, S. (2011). Phytophthora infestans effector AVRblb2 prevents secretion of a plant immune protease at the haustorial interface. *Proceedings of the National Academy of Sciences of the United States of America*, *108*(51), 20832–20837. https://doi.org/10.1073/pnas.1112708109

Brown, I., Trethowan, J., Kerry, M., Mansfield, J., & Bolwell, G. P. (1998). Localization of components of the oxidative cross-linking of glycoproteins and of callose synthesis in papillae formed during the interaction between non-pathogenic strains of Xanthomonas campestris and French bean mesophyll cells. *The Plant Journal*, *15*(3), 333–343. https://doi.org/10.1046/J.1365-313X.1998.00215.X

Brunkard, J. O., Runkel, A. M., & Zambryski, P. C. (2015). Chloroplasts extend stromules independently and in response to internal redox signals. *Proceedings of the National Academy of Sciences of the United States of America*, *112*(32), 10044–10049. https://doi.org/10.1073/pnas.1511570112

Caillaud, M.-C., Piquerez, S. J. M., Fabro, G., Steinbrenner, J., Ishaque, N., Beynon, J., & Jones, J. D. G. (2012). Subcellular localization of the Hpa RxLR effector repertoire identifies a tonoplast-associated protein HaRxL17 that confers enhanced plant susceptibility. *The Plant Journal*, *69*(2), 252–265. https://doi.org/10.1111/J.1365-313X.2011.04787.X

Caillaud, M.-C., Wirthmueller, L., Sklenar, J., Findlay, K., Piquerez, S. J. M., Jones, A. M. E., Robatzek, S., Jones, J. D. G., & Faulkner, C. (2014). The Plasmodesmal Protein PDLP1 Localises to Haustoria-Associated Membranes during Downy Mildew Infection and Regulates Callose Deposition. *PLOS Pathogens*, *10*(11), e1004496. https://doi.org/10.1371/JOURNAL.PPAT.1004496

Caplan, J. L., Kumar, A. S., Park, E., Padmanabhan, M. S., Hoban, K., Modla, S., Czymmek, K., & Dinesh-Kumar, S. P. (2015). Chloroplast Stromules Function during Innate Immunity. *Developmental Cell*, *34*(1), 45–57. https://doi.org/10.1016/j.devcel.2015.05.011

Chaparro-Garcia, A., Schwizer, S., Sklenar, J., Yoshida, K., Petre, B., Bos, J. I. B., Schornack, S., Jones, A. M. E., Bozkurt, T. O., & Kamoun, S. (2015). Phytophthora infestans RXLR-WY effector AVR3a associates with dynamin-related protein 2 required for endocytosis of the plant pattern recognition receptor FLS2. *PLoS ONE*, *10*(9), e0137071. https://doi.org/10.1371/journal.pone.0137071

Dagdas, Y. F., Pandey, P., Tumtas, Y., Sanguankiattichai, N., Belhaj, K., Duggan, C., Leary, A. Y., Segretin, M. E., Contreras, M. P., Savage, Z., Khandare, V. S., Kamoun, S., & Bozkurt, T. O. (2018). Host autophagy machinery is diverted to the pathogen interface to mediate focal defense responses against the irish potato famine pathogen. *ELife*, *7*, 1–15. https://doi.org/10.7554/eLife.37476

Daniel, R., & Guest, D. (2005). Defence responses induced by potassium phosphonate in Phytophthora palmivora-challenged Arabidopsis thaliana. *Physiological and Molecular Plant Pathology*, *67*(3–5), 194–201. https://doi.org/10.1016/J.PMPP.2006.01.003

Daudi, A., Cheng, Z., O'Brien, J. A., Mammarella, N., Khan, S., Ausubel, F. M., & Bolwell, G. P. (2012). The apoplastic oxidative burst peroxidase in Arabidopsis is a major component of pattern-triggered immunity. *The Plant Cell*, *24*(1), 275–287. https://doi.org/10.1105/TPC.111.093039

Davis, A. M., Hall, A., Millar, A. J., Darrah, C., & Davis, S. J. (2009). Protocol: Streamlined sub-protocols for floral-dip transformation and selection of transformants in Arabidopsis thaliana. *Plant Methods 2009 5:1*, *5*(1), 1–7. https://doi.org/10.1186/1746-4811-5-3

Ding, X., Jimenez-Gongora, T., Krenz, B., & Lozano-Duran, R. (2019). Chloroplast clustering around the nucleus is a general response to pathogen perception in Nicotiana benthamiana. *Molecular Plant Pathology*, *20*(9), 1298–1306. https://doi.org/10.1111/mpp.12840

Duggan, C., Moratto, E., Savage, Z., Hamilton, E., Adachi, H., Wu, C.-H., Leary, A. Y., Tumtas, Y., Rothery, S. M., Maqbool, A., Nohut, S., Martin, T. R., Kamoun, S., & Bozkurt, T. O. (2021). Dynamic localization of a helper NLR at the plant–pathogen interface underpins pathogen recognition. *Proceedings of the National Academy of Sciences*, *118*(34), e2104997118. https://doi.org/10.1073/PNAS.2104997118

Ellinger, D., Naumann, M., Falter, C., Zwikowics, C., Jamrow, T., Manisseri, C., Somerville, S. C., & Voigt, C. A. (2013). Elevated Early Callose Deposition Results in Complete Penetration Resistance to Powdery Mildew in Arabidopsis. *Plant Physiology*, *161*(3), 1433–1444. https://doi.org/10.1104/PP.112.211011

Erickson, J. L., Adlung, N., Lampe, C., Bonas, U., & Schattat, M. H. (2018). The Xanthomonas effector XopL uncovers the role of microtubules in stromule extension and dynamics in Nicotiana benthamiana. *Plant Journal*, *93*(5), 856–870. https://doi.org/10.1111/tpj.13813

Erickson, J. L., Kantek, M., & Schattat, M. H. (2017). Plastid-Nucleus Distance Alters the Behavior of Stromules. *Frontiers in Plant Science*, *0*, 1135. https://doi.org/10.3389/FPLS.2017.01135

Erickson, J. L., Ziegler, J., Guevara, D., Abel, S., Klösgen, R. B., Mathur, J., Rothstein, S. J., & Schattat, M. H. (2014). Agrobacterium-derived cytokinin influences plastid morphology and starch accumulation in Nicotiana benthamiana during transient assays. *BMC Plant Biology*, *14*(1), 127. https://doi.org/10.1186/1471-2229-14-127

Foyer, C. H., & Noctor, G. (2003). Redox sensing and signalling associated with reactive oxygen in chloroplasts, peroxisomes and mitochondria. *Physiologia Plantarum*, *119*(3), 355–364. https://doi.org/10.1034/J.1399-3054.2003.00223.X

Freytag, S., Arabatzis, N., Hahlbrock, K., & Schmelzer, E. (1994). Reversible cytoplasmic rearrangements precede wall apposition, hypersensitive cell death and defense-related gene activation in potato/Phytophthora infestans interactions. *Source: Planta*, *194*(1), 123–135. https://www.jstor.org/stable/23383035

Fuchs, R., Kopischke, M., Klapprodt, C., Hause, G., Meyer, A. J., Schwarzländer, M., Fricker, M. D., & Lipka, V. (2016). Immobilized Subpopulations of Leaf Epidermal Mitochondria Mediate PENETRATION2-Dependent Pathogen Entry Control in Arabidopsis. *The Plant Cell*, *28*(1), 130–145. https://doi.org/10.1105/TPC.15.00887

Gao, C., Xu, H., Huang, J., Sun, B., Zhang, F., Savage, Z., Duggan, C., Yan, T., Wu, C., Wang, Y., Vleeshouwers, V. G. A. A., Kamoun, S., Bozkurt, T. O., & Dong, S. (2020). Pathogen manipulation of chloroplast function triggers a light-dependent immune recognition. *Proceedings of the National Academy of Sciences*, *117*(17), 9613–9620. https://doi.org/10.1073/PNAS.2002759117

Gibson, D. G., Young, L., Chuang, R.-Y., Venter, J. C., Hutchison, C. A., & Smith, H. O. (2009). Enzymatic assembly of DNA molecules up to several hundred kilobases. *Nature Methods*, *6*(5), 343–345. https://doi.org/10.1038/NMETH.1318

Goldfarb, D. S., Gariépy, J., Schoolnik, G., & Kornberg, R. D. (1986). Synthetic peptides as nuclear localization signals. *Nature 1986 322:6080*, *322*(6080), 641–644. https://doi.org/10.1038/322641a0

Guest, D. I. (1986). Evidence from light microscopy of living tissues that Fosetyl-Al modifies the defence response in tobacco seedlings following inoculation by Phytophthora nicotianae var nicotianae. *Physiological and Molecular Plant Pathology*, *29*(2), 251–261. https://doi.org/10.1016/S0048-4059(86)80025-X

Heath, M. C., Nimchuk, Z. L., & Xu, H. (1997). Plant nuclear migrations as indicators of critical interactions between resistant or susceptible cowpea epidermal cells and invasion hyphae of the cowpea rust fungus. *The New Phytologist*, *135*(4), 689–700. https://doi.org/10.1046/J.1469-8137.1997.00710.X

Hellens, R., Mullineaux, P., & Klee, H. (2000). Technical Focus:a guide to Agrobacterium binary Ti vectors. *Trends in Plant Science*, *5*(10), 446–451. https://doi.org/10.1016/S1360-1385(00)01740-4

Higa, T., Suetsugu, N., Kong, S. G., & Wada, M. (2014). Actin-dependent plastid movement is required for motive force generation in directional nuclear movement in plants. *Proceedings of the National Academy of Sciences of the United States of America*, *111*(11), 4327–4331. https://doi.org/10.1073/pnas.1317902111

Irieda, H., & Takano, Y. (2021). Epidermal chloroplasts are defense-related motile organelles equipped with plant immune components. *Nature Communications 2021 12:1*, *12*(1), 1–19. https://doi.org/10.1038/s41467-021-22977-5

Jelenska, J., Yao, N., Vinatzer, B. A., Wright, C. M., Brodsky, J. L., & Greenberg, J. T. (2007). A J Domain Virulence Effector of Pseudomonas syringae Remodels Host Chloroplasts and Suppresses Defenses. *Current Biology*, *17*(6), 499–508. https://doi.org/10.1016/j.cub.2007.02.028

Klösgen, R. B., & Schattat, M. H. (2009). Improvement of plant cell microscope images by use of 'Depth of Field' - extending software. *Endocytobiosis and Cell Research*, *19*, 11–19.

Koh, S., André, A., Edwards, H., Ehrhardt, D., & Somerville, S. (2005). Arabidopsis thaliana subcellular responses to compatible Erysiphe cichoracearum infections. *Plant Journal*, *44*(3), 516–529. https://doi.org/10.1111/j.1365-313X.2005.02545.x

Kumar, A. S., Park, E., Nedo, A., Alqarni, A., Ren, L., Hoban, K., Modla, S., McDonald, J. H., Kambhamettu, C., Dinesh-Kumar, S. P., & Caplan, J. L. (2018). Stromule extension along microtubules coordinated with actin-mediated anchoring guides perinuclear chloroplast movement during innate immunity. *ELife*, *7*, 1–33. https://doi.org/10.7554/eLife.23625

Kwok, E. Y., & Hanson, M. R. (2004). Plastids and stromules interact with the nucleus and cell membrane in vascular plants. *Plant Cell Reports*, *23*(4), 188–195. https://doi.org/10.1007/s00299-004-0824-9

Kwon, C., Neu, C., Pajonk, S., Yun, H. S., Lipka, U., Humphry, M., Bau, S., Straus, M., Kwaaitaal, M., Rampelt, H., Kasmi, F. El, Jürgens, G., Parker, J., Panstruga, R., Lipka, V., & Schulze-Lefert, P. (2008). Co-option of a default secretory pathway for plant immune responses. *Nature*, *451*(7180), 835–840. https://doi.org/10.1038/nature06545

Littlejohn, G. R., Breen, S., Smirnoff, N., & Grant, M. (2021). Chloroplast immunity illuminated. *New Phytologist*, *229*(6), 3088–3107. https://doi.org/10.1111/NPH.17076

Micali, C. O., Neumann, U., Grunewald, D., Panstruga, R., & O'Connell, R. (2011). Biogenesis of a specialized plant–fungal interface during host cell internalization of Golovinomyces orontii haustoria. *Cellular Microbiology*, *13*(2), 210–226. https://doi.org/10.1111/J.1462-5822.2010.01530.X

O'brien, J. A., Daudi, A., Butt, V. S., & Paul Bolwell, G. (2012). *Reactive oxygen species and their role in plant defence and cell wall metabolism*. *236*(3), 765–779. https://about.jstor.org/terms

Oikawa, K., Kasahara, M., Kiyosue, T., Kagawa, T., Suetsugu, N., Takahashi, F., Kanegae, T., Niwa, Y., Kadota, A., & Wada, M. (2003). Chloroplast Unusual Positioning1 Is Essential for Proper Chloroplast Positioning. *Plant Cell*, *15*(12), 2805–2815. https://doi.org/10.1105/tpc.016428

Oikawa, K., Yamasato, A., Kong, S. G., Kasahara, M., Nakai, M., Takahashi, F., Ogura, Y., Kagawa, T., & Wada, M. (2008). Chloroplast outer envelope protein Chup1 is essential for chloroplast anchorage to the plasma membrane and chloroplast movement. *Plant Physiology*, *148*(2), 829–842. https://doi.org/10.1104/pp.108.123075

Pecrix, Y., Buendia, L., Penouilh-Suzette, C., Maréchaux, M., Legrand, L., Bouchez, O., Rengel, D., Gouzy, J., Cottret, L., Vear, F., & Godiard, L. (2019). Sunflower resistance to multiple downy mildew pathotypes revealed by recognition of conserved effectors of the oomycete Plasmopara halstedii. *Plant Journal*, *97*(4), 730–748. https://doi.org/10.1111/tpj.14157

Petre, B., Lorrain, C., Saunders, D. G. O., Win, J., Sklenar, J., Duplessis, S., & Kamoun, S. (2016). Rust fungal effectors mimic host transit peptides to translocate into chloroplasts. *Cellular Microbiology*, *18*(4), 453–465. https://doi.org/10.1111/cmi.12530

Prinz, W. A., Toulmay, A., & Balla, T. (2019). The functional universe of membrane contact sites. *Nature Reviews Molecular Cell Biology 2019 21:1*, *21*(1), 7–24. https://doi.org/10.1038/s41580-019-0180-9

Radojičić, A., Li, X., & Zhang, Y. (2018). Salicylic acid: A double-edged sword for programed cell death in plants. *Frontiers in Plant Science*, *9*(August), 1–5. https://doi.org/10.3389/fpls.2018.01133

Rodríguez-Herva, J. J., González-Melendi, P., Cuartas-Lanza, R., Antúnez-Lamas, M., Río-Alvarez, I., Li, Z., López-Torrejón, G., Díaz, I., Pozo, J. C. del, Chakravarthy, S., Collmer, A., Rodríguez-Palenzuela, P., & López-Solanilla, E. (2012). A bacterial cysteine protease effector protein interferes with photosynthesis to suppress plant

innate immune responses. *Cellular Microbiology*, *14*(5), 669–681. https://doi.org/10.1111/J.1462-5822.2012.01749.X

Savage, Z., Duggan, C., Toufexi, A., Pandey, P., Liang, Y., Segretin, M. E., Yuen, L. H., Gaboriau, D. C. A., Leary, A. Y., Tumtas, Y., Khandare, V., Ward, A. D., Botchway, S. W., Bateman, B. C., Pan, I., Schattat, M., Sparkes, I., & Bozkurt, T. O. (2021). Chloroplasts alter their morphology and accumulate at the pathogen interface during infection by Phytophthora infestans. *The Plant Journal*. https://doi.org/10.1111/TPJ.15416

Schattat, M., Barton, K., Baudisch, B., Klösgen, R. B., & Mathur, J. (2011). Plastid stromule branching coincides with contiguous endoplasmic reticulum dynamics. *Plant Physiology*, *155*(4), 1667–1677. https://doi.org/10.1104/pp.110.170480

Schmelzer, E. (2002). Cell polarization, a crucial process in fungal defence. *Trends in Plant Science*, *7*(9), 411–415. https://doi.org/10.1016/S1360-1385(02)02307-5

Schneider, C. A., Rasband, W. S., & Eliceiri, K. W. (2012). NIH Image to ImageJ: 25 years of image analysis. In *Nature Methods* (Vol. 9, Issue 7, pp. 671–675). Nature Publishing Group. https://doi.org/10.1038/nmeth.2089

Shapiguzov, A., Vainonen, J. P., Wrzaczek, M., & Kangasjärvi, J. (2012). ROS-talk - how the apoplast, the chloroplast, and the nucleus get the message through. *Frontiers in Plant Science*, *3*(DEC), 1–9. https://doi.org/10.3389/fpls.2012.00292

Sheahan, M. B., Collings, D. A., Rose, R. J., & McCurdy, D. W. (2020). ACTIN7 is required for perinuclear clustering of chloroplasts during arabidopsis protoplast culture. *Plants*, *9*(2). https://doi.org/10.3390/plants9020225

Sheahan, M. B., Rose, R. J., & McCurdy, D. W. (2004). Organelle inheritance in plant cell division: The actin cytoskeleton is required for unbiased inheritance of chloroplasts, mitochondria and endoplasmic reticulum in dividing protoplasts. *Plant Journal*, *37*(3), 379–390. https://doi.org/10.1046/j.1365-313X.2003.01967.x

Singh, R., Lee, S., Ortega, L., Ramu, V. S., Muthappa Senthil-Kumar, Blancaflor, E. B., Rojas, C. M., & Mysore, K. S. (2018). Two Chloroplast-Localized Proteins: AtNHR2A and AtNHR2B, Contribute to Callose Deposition During Nonhost Disease Resistance in Arabidopsis. *Molecular Plant-Microbe Interactions : MPMI*, *31*(12), 1280–1290. https://doi.org/10.1094/MPMI-04-18-0094-R

Stuttmann, J., Barthel, K., Martin, P., Ordon, J., Erickson, J. L., Herr, R., Ferik, F., Kretschmer, C., Berner, T., Keilwagen, J., Marillonnet, S., & Bonas, U. (2021). Highly efficient multiplex editing: one-shot generation of 8× Nicotiana benthamiana and 12× Arabidopsis mutants. *The Plant Journal*, *106*(1), 8–22. https://doi.org/10.1111/TPJ.15197

Su, J., Yang, L., Zhu, Q., Wu, H., He, Y., Liu, Y., Xu, J., Jiang, D., & Zhang, S. (2018). Active photosynthetic inhibition mediated by MPK3/MPK6 is critical to effector-triggered immunity. *PLoS Biology*, *16*(5), 1–29. https://doi.org/10.1371/journal.pbio.2004122

Suetsugu, N., Higa, T., Gotoh, E., & Wada, M. (2016). Light-induced movements of chloroplasts and nuclei are regulated in both cp-actin-filament-dependent and -independent manners in arabidopsis thaliana. *PLoS ONE*, *11*(6), e0157429. https://doi.org/10.1371/journal.pone.0157429

Thordal-Christensen, H., Zhang, Z., Wei, Y., & Collinge, D. B. (1997). Subcellular localization of H2O2 in plants. H2O2 accumulation in papillae and hypersensitive response during the barley—powdery mildew interaction. *The Plant Journal*, *11*(6), 1187–1194. https://doi.org/10.1046/J.1365-313X.1997.11061187.X

Wada, M., & Kong, S. G. (2018). Actin-mediated movement of chloroplasts. In *Journal of Cell Science* (Vol. 131, Issue 2). Company of Biologists Ltd. https://doi.org/10.1242/jcs.210310

Wang, S., Boevink, P. C., Welsh, L., Zhang, R., Whisson, S. C., & Birch, P. R. J. (2017). Delivery of cytoplasmic and apoplastic effectors from Phytophthora infestans haustoria by distinct secretion pathways. *New Phytologist*. https://doi.org/10.1111/nph.14696

Wang, X., Sager, R., Cui, W., Zhang, C., Lu, H., & Lee, J. Y. (2013). Salicylic acid regulates plasmodesmata closure during innate immune responses in Arabidopsis. *Plant Cell*, *25*(6), 2315–2329. https://doi.org/10.1105/tpc.113.110676

Wellburn, A. R. (1994). The Spectral Determination of Chlorophylls a and b, as well as Total Carotenoids, Using Various Solvents with Spectrophotometers of Different Resolution. *Journal of Plant Physiology*, *144*(3), 307–313. https://doi.org/10.1016/S0176-1617(11)81192-2

Whisson, S. C., Boevink, P. C., Moleleki, L., Avrova, A. O., Morales, J. G., Gilroy, E. M., Armstrong, M. R., Grouffaud, S., Van West, P., Chapman, S., Hein, I., Toth, I. K., Pritchard, L., & Birch, P. R. J. (2007). A translocation signal for delivery of oomycete effector proteins into host plant cells. *Nature*, *450*(7166), 115–118. https://doi.org/10.1038/nature06203

Xu, Q., Tang, C., Wang, X., Sun, S., Zhao, J., Kang, Z., & Wang, X. (2019). An effector protein of the wheat stripe rust fungus targets chloroplasts and suppresses chloroplast function. *Nature Communications 2019 10:1*, *10*(1), 1–13. https://doi.org/10.1038/s41467-019-13487-6

Yang, K.-Y., Liu, Y., & Zhang, S. (2001). Activation of a mitogen-activated protein kinase pathway is involved in disease resistance in tobacco. *Proceedings of the National Academy of Sciences*, *98*(2), 741–746. https://doi.org/10.1073/PNAS.98.2.741

Zabala, M. de T., Littlejohn, G., Jayaraman, S., Studholme, D., Bailey, T., Lawson, T., Tillich, M., Licht, D., Bölter, B., Delfino, L., Truman, W., Mansfield, J., Smirnoff, N., & Grant, M. (2015). Chloroplasts play a central role in plant defence and are targeted by pathogen effectors. *Nature Plants*, *1*(6), 15074. https://doi.org/10.1038/NPLANTS.2015.74

Zurbriggen, M. D., Carrillo, N., Tognetti, V. B., Melzer, M., Peisker, M., Hause, B., & Hajirezaei, M.-R. (2009). Chloroplast-generated reactive oxygen species play a major role in localized cell death during the non-host interaction between tobacco and Xanthomonas campestris pv. vesicatoria. *The Plant Journal*, *60*(6), 962–973. https://doi.org/10.1111/J.1365-313X.2009.04010.X

SUPPLEMENTARY

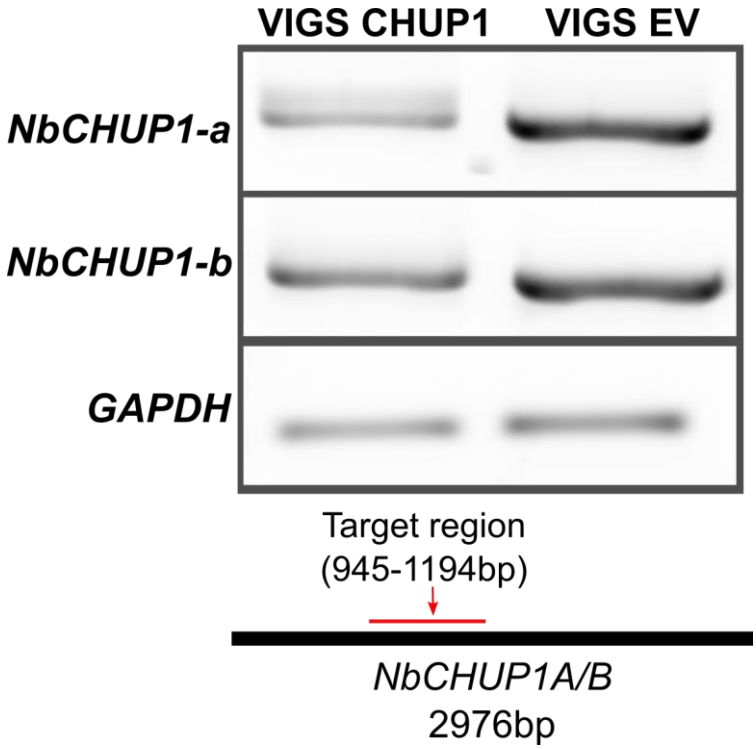

Supplementary figure 1: 12 day old transplastomic CpGFP N. benthamiana plants, were infiltrated with Agrobacterium expressing VIGS CHUP1 or VIGS EV constructs. Leaf disks were taken from 5-week old, uninfected, silenced tissue and RNA was extracted. Semi-quantitative RT-PCR of *CHUP1* shows that it was silenced in VIGS CHUP1 tissue compared to EV. RT-PCR of housekeeping GAPDH was used as an internal control for cDNA loading.

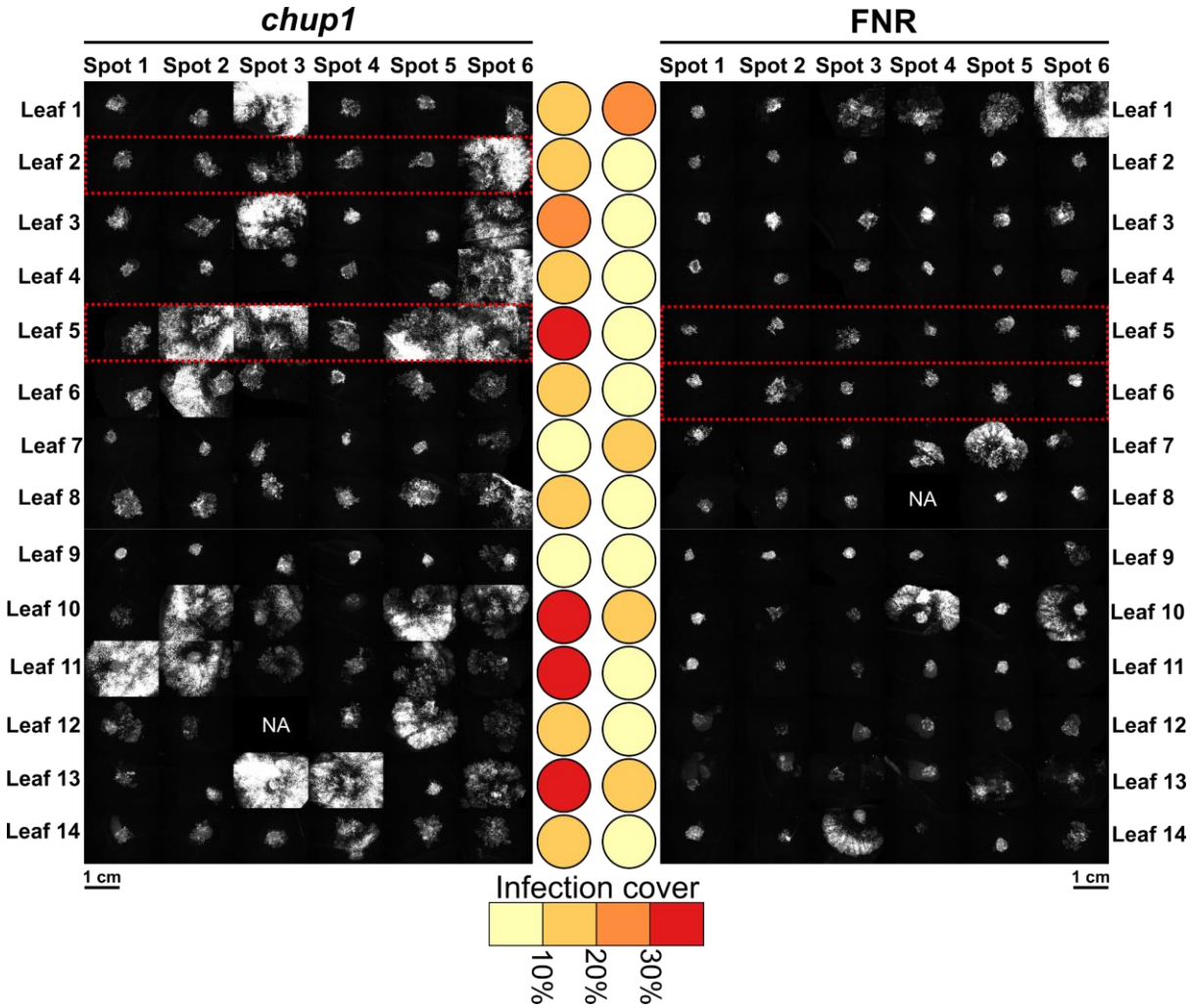

Supplementary figure 2: Extended infection assay data for Figure 1A.

Hyphal growth assays of *chup1* and FNR plants infected with *P. infestans* 88069td and imaged by fluorescence stereomicroscopy five days post inoculation. Each leaf was inoculated with six droplets of spore solution (labelled here as spots), all data shown. Percentage of image covered by hyphae calculated for each leaf (across all six inoculation spots) and displayed by color, where red are the strongest infections. Red dashed boxes mark data presented in main text Figure 1A.

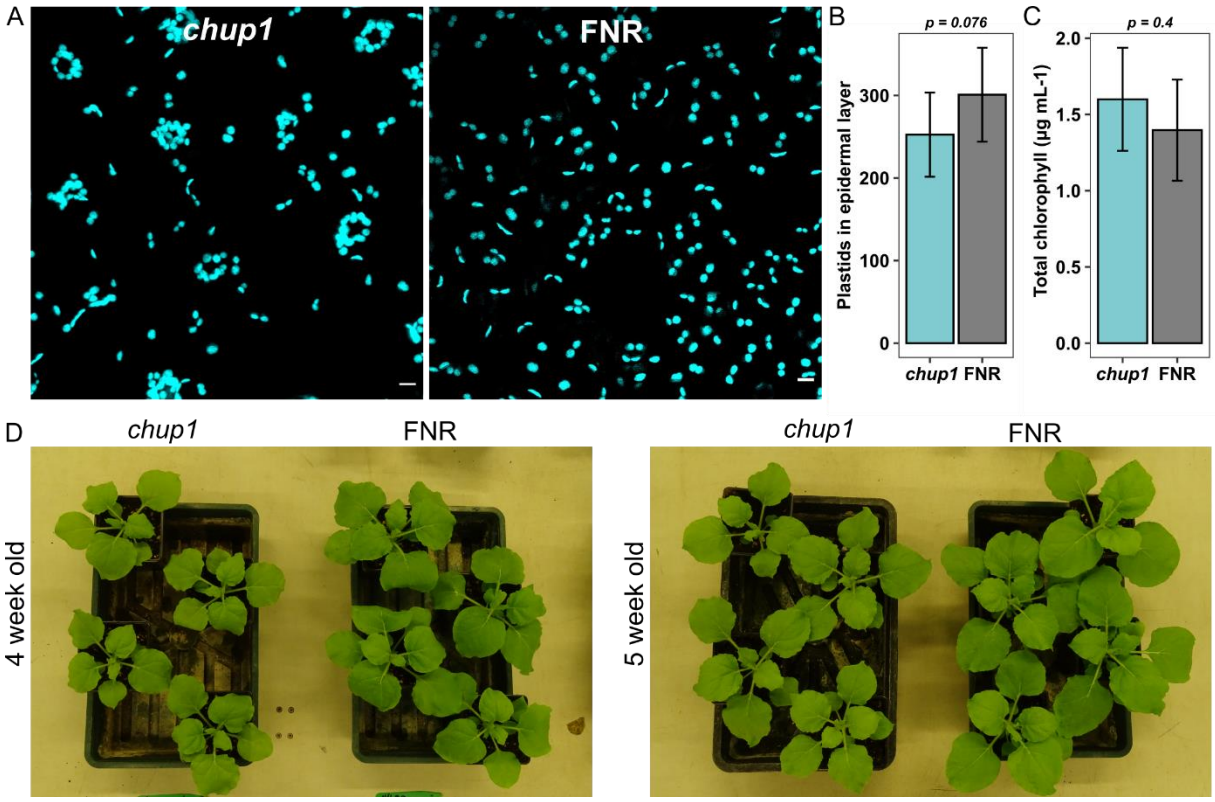

Supplementary figure 3: Chlorophyll concentration and plastid counts are similar in the *chup1* and FNR plants.

(A) Maximum projection confocal micrographs of *chup1* and FNR where the entire depth of the epidermal layer is shown. Images have been intentionally and openly doctored to remove sections containing guard and mesophyll cells show only the epidermal chloroplasts. (B) Quantification of hand counted chloroplasts in the epidermal layer of nine images for each *chup1* and FNR plants. Error bars show standard deviation, *p*-value calculated from Student's T test. (C) Total chlorophyll concentration of *chup1* and FNR samples (three per genotype). Error bars show standard deviation, *p*-value calculated from Wilcoxon test. (D) Photographs of representative *chup1* and FNR plants used for experiments at four and five weeks old.

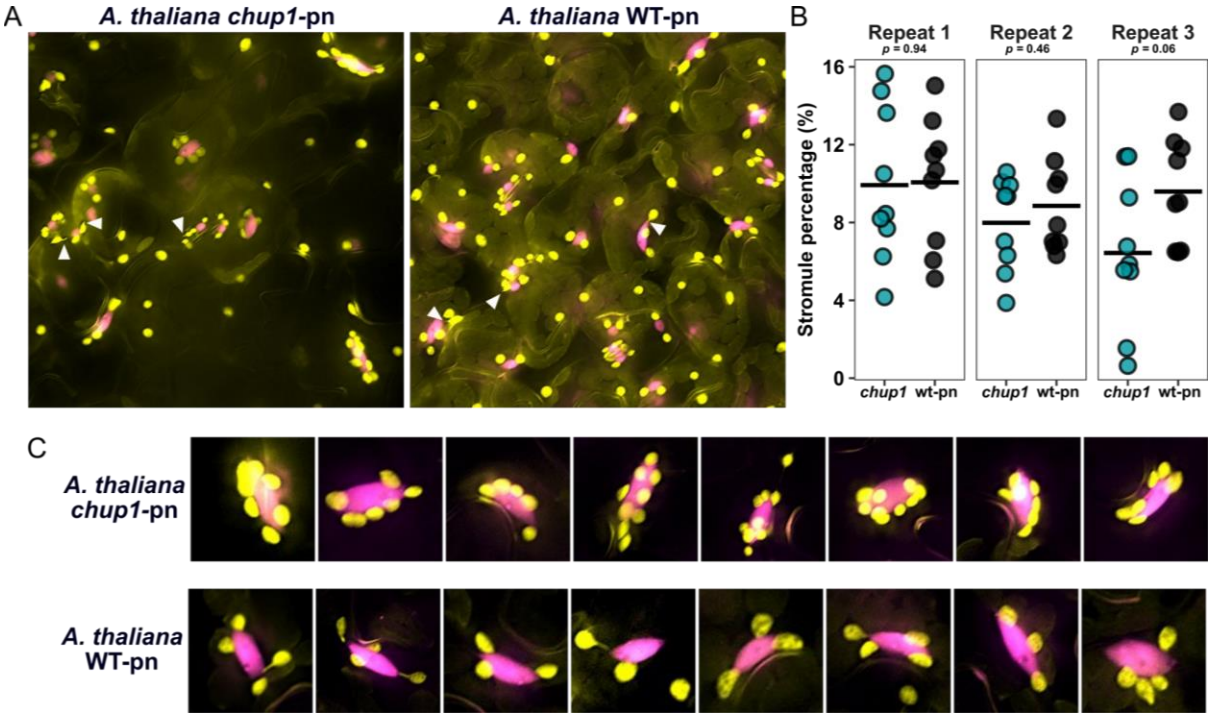

Supplementary figure 4: *A. thaliana chup1* knock-out lines do not have significantly fewer stromules than control lines, but do show constitutive perinuclear plastid clustering.

(A) Widefield fluorescence microscopy images of *A. thaliana chup1*-pn and control WT-pn plants. Where both lines express GFP in the stroma (yellow) and mCherry in the nucleus (magenta). (B) Quantification of stromule percentage in untreated *A. thaliana chup1*-pn and control WT-pn plants across three separate replicates, where each replicate is an independently generated transgenic line. (C) Isolated nuclei from *A. thaliana chup1*-pn and control WT-pn plants showing differing amounts of perinuclear plastid clustering. Yellow = stroma GFP, magenta = nuclear localized mCherry.

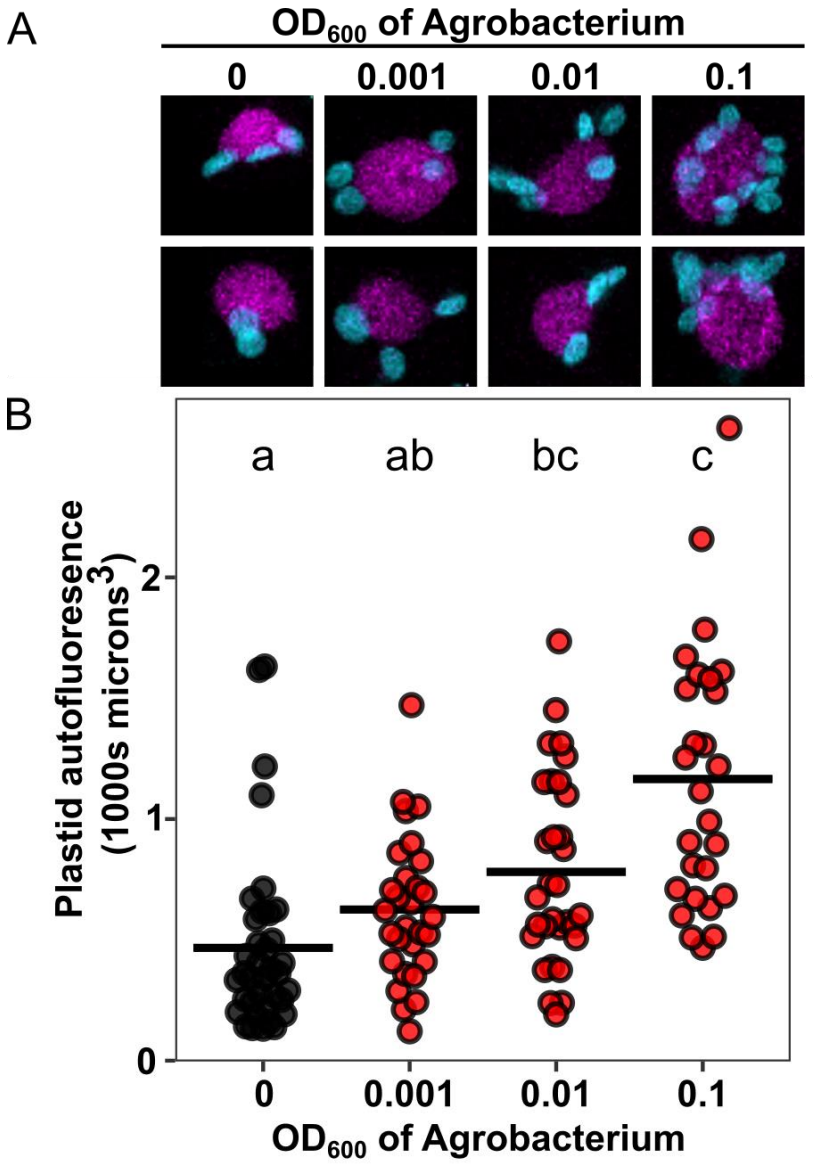

Supplementary figure 5: GV3101 causes perinuclear clustering.
(A) Maximum projection confocal micrographs of nuclei in transgenic *N. benthamiana* where the nucleus is labelled with mCherry (magenta here), and the stroma with GFP (not shown). Cyan shows chloroplast autofluorescence. Plants infiltrated with varying optical densities of *A. tumefaciens* GV3101, here expressing NLS-BFP (channel not shown) . OD_{600} of 0 means agroinfiltration buffer only was infiltrated. Scale bars are 10 μm. (B) Automated quantifications of volume (microns cubed) of chloroplast autofluorescence surrounding nuclei marked from image set exemplified in A, infiltrated with varying optical densities of *A. tumefaciens* GV3101. Cross bar represents group mean, significance groups shown by letters and calculated by Dunn's test. Each data point represents measurement from a single isolated nucleus.

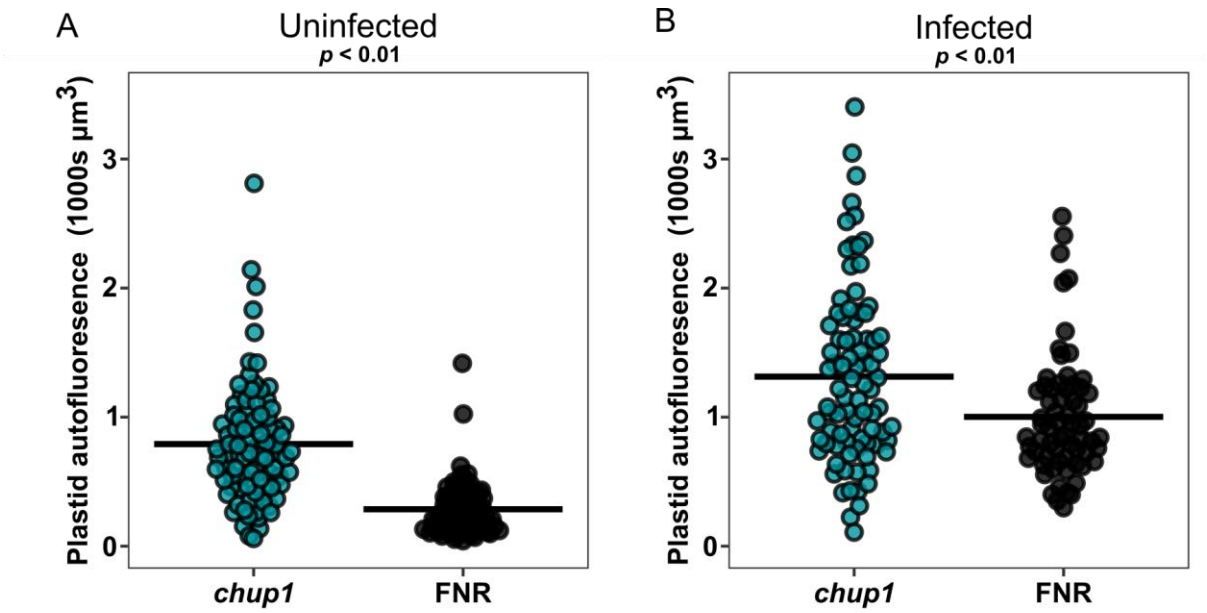

Supplementary figure 6: Infection causes greater perinuclear clustering in both *chup1* and FNR plants.

Automated quantifications of volume (microns cubed) of chloroplast autofluorescence surrounding nuclei marked by NLS-BFP in *chup1* and FNR plants either uninfected (left) or infected with *P. infestans* 88069td, three days post inoculation (right). Uninfected data (left) shown in main text Figure 4C, but shown again here for easier comparison to the infected data set. For both, data has been collated together from three independent plants, and infections (where relevant), for simpler plotting. Cross bar represents group mean, significance groups shown by letters and calculated by Wilcoxon test. Each data point represents measurement from a single isolated nucleus.

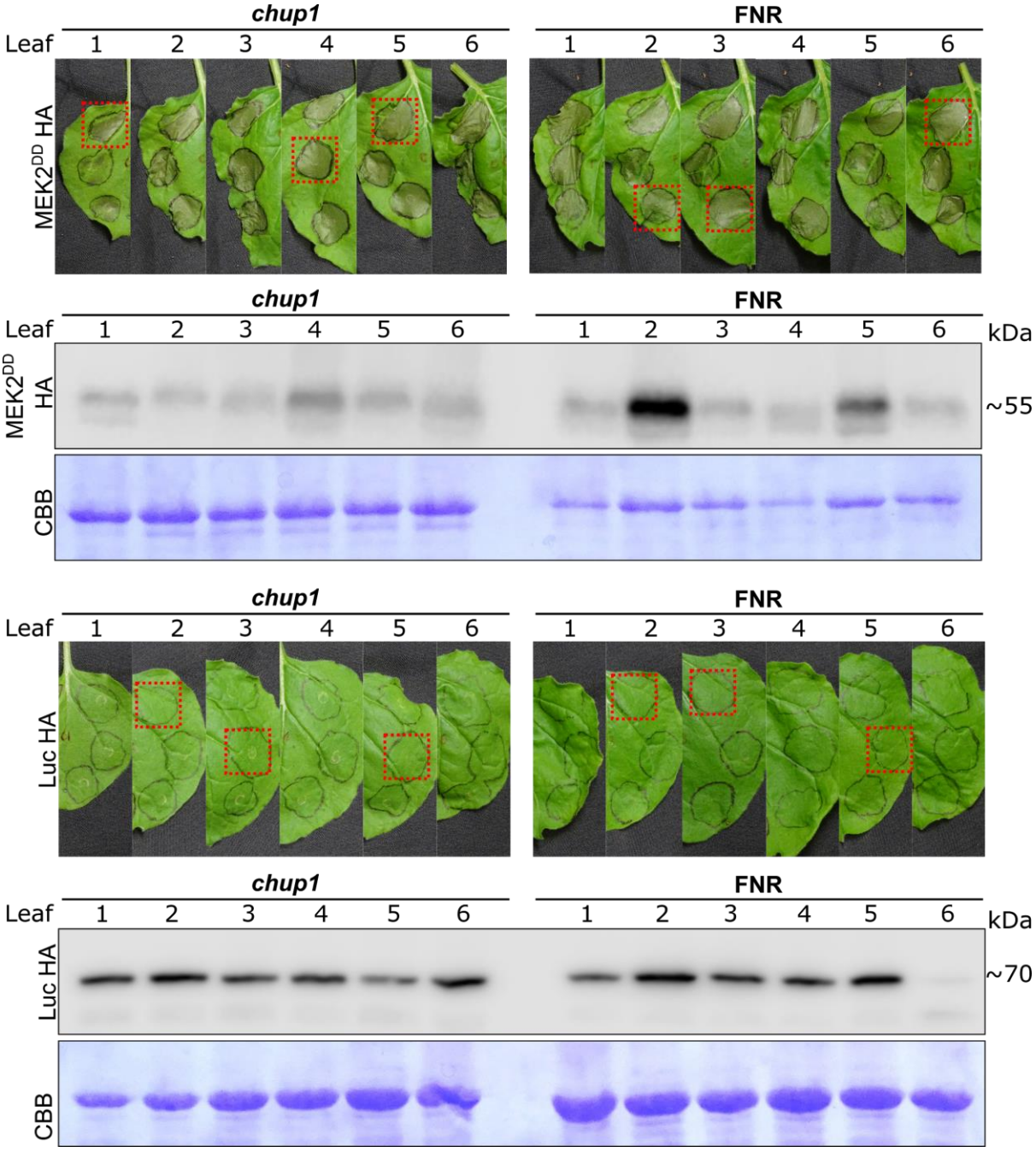

Supplementary figure 7: Extended MEK2DD cell death data for Figure 5E.

Cell death assay following transient expression of MEK2^{DD} 3xHA or Luciferase (Luc) 3xHA control. Photographs of infiltrated tissue were taken three days post infiltration. All data shown. Red dashed boxes mark data presented in main text Figure 5E. Western blot detection of HA tagged constructs. Samples taken from the infiltrated regions of the same leaves photographed for cell death that are also shown here. CBB = coomassie brilliant blue staining of gel post transfer of proteins shown for loading control.

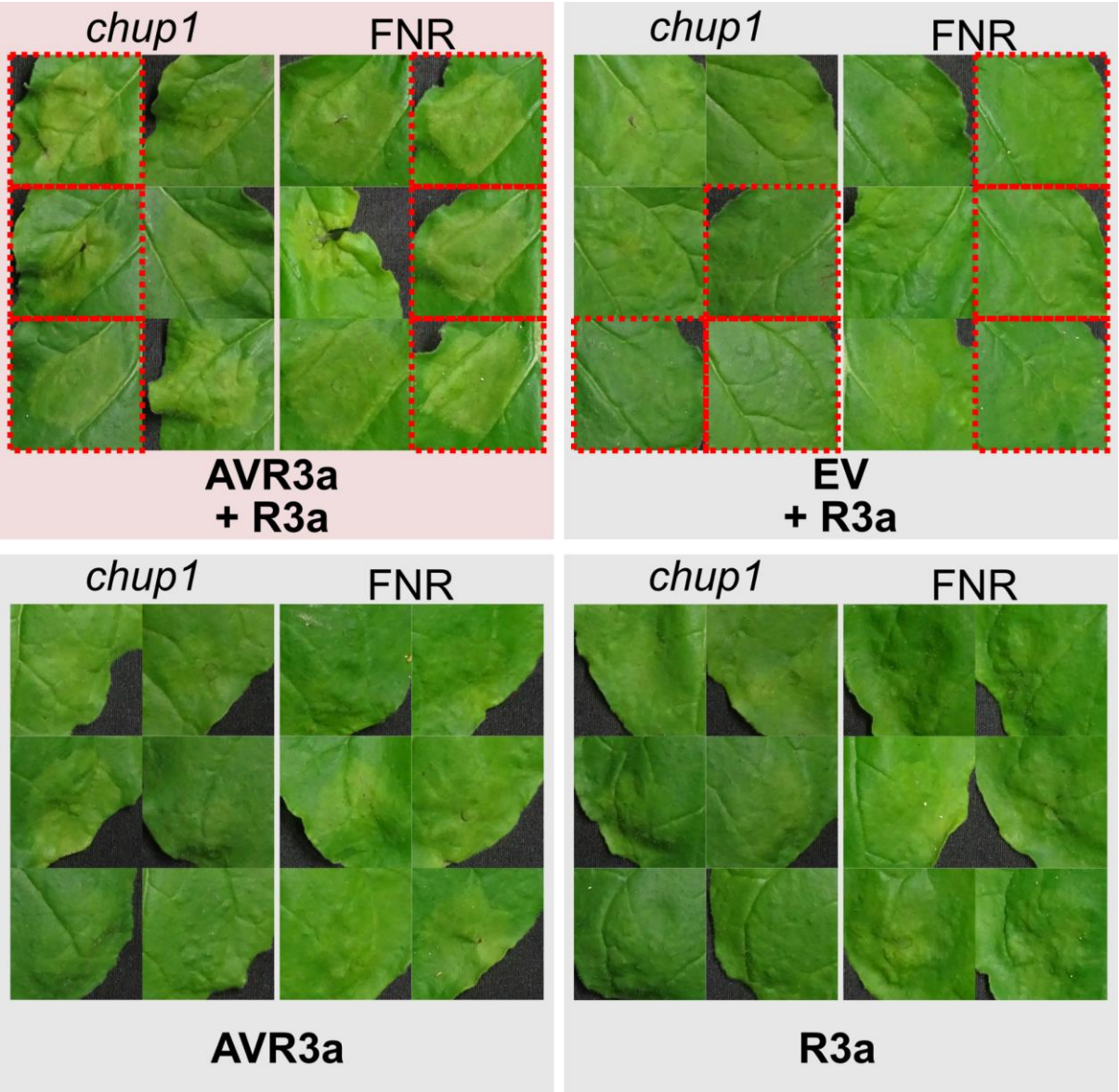

Supplementary figure 8: Extended R3a/AVR3a cell death data for Figure 5F.
Cell death assay following transient co-expression of R3a with AVR3a or empty vector control as well as R3a and AVR3a expressed alone. Photographs of infiltrated tissue were taken three days post infiltration. All data shown. Red dashed boxes mark data presented in main text Figure 5F.